Supplement of Atmos. Chem. Phys., 26, 6683–6702, 2026
https://doi.org/10.5194/acp-26-6683-2026-supplement

Atmospheric Chemistry and Physics
Open Access

Supplement of

Contrasting air pollution responses to hourly varying anthropogenic NO_x emissions in the contiguous United States

Madankui Tao et al.

Correspondence to: Madankui Tao (taoma528@mit.edu)

Text S1. Interpreting the *BASE* Case: Sensitivity to Emissions Perturbations and Alternative Chemistry

To optimize computational resources while still identifying key sensitivities, we perform five simulations over five days from July 1 to July 5, 2018 (Table S1). We conduct three simulations to evaluate model responses to major sources of precursors, including 1) a 30% reduction in total anthropogenic emissions (hereafter referred to as *CAMS_m30anthro*) by modifying the anthropogenic emissions files; 2) a 30% reduction in total biogenic emissions (*CAMS_m30bio*) by scaling MEGAN emission factors to 0.7; and 3) the implementation of the MOZART-TS2 chemical mechanism (*CAMS_chemTS2*) by changing the model component set, which incorporates more comprehensive gas-phase chemistry for isoprene and terpenes (Schwantes et al., 2022). Analysis of these simulations provides context for evaluating changes in concentrations and chemical sensitivity driven by the incorporation of the regional 2017 U.S. National Emissions Inventory (NEI) adjusted for July 2018 simulation and by differences in the temporal resolution of anthropogenic emissions. The selected 30% perturbation for emission sources allows us to detect signals while maintaining relevance for scaling linearly to 100% (Turnock et al., 2018; Wild et al., 2012; Wu et al., 2009).

Overall, the emission perturbation simulations indicate that pollutants decrease with reductions of their dominant sources, as expected. A 30% reduction in total anthropogenic emissions leads to regional average decreases in all pollutants: surface NO_2 concentrations decrease by 20-24% (0.3-0.6 ppb; range reflects the average concentrations in six different regions indicated in Fig. 1), O_3 by 2.6-7.5% (1.1-3.5 ppb), HCHO by about 5.0% (0.1-0.4 ppb), CO by 3.1-6.6% (3.7-10 ppb), SO_2 by 19-25% (0.1-0.6 ppb), and $PM_{2.5}$ by 1.7-5.4% (0.1-0.7 μg/m^3) (Figs. S1 and S2). The largest reductions in NO_2 and CO occur in areas where emissions of these pollutants are largest (Fig. S4b). The Northeast region shows the largest decreases in O_3, surface NO_2 and HCHO, while the western CONUS experiences the smallest reductions (Fig. S1). On the other hand, a 30% reduction in biogenic emissions leads to greater changes in HCHO concentrations compared to a 30% reduction in anthropogenic emissions, with regional mean decreases of 8.2-19% (0.1-1.1 ppb). Surface CO concentrations also decrease by 1.4-6.2% (1.3-10 ppb), indicating similar ranges of sensitivity to biogenic and anthropogenic emissions. The most substantial reductions in

HCHO and CO occur in the eastern CONUS, where the spatial pattern aligns most closely with biogenic isoprene emissions, which are significantly higher than those of other biogenic VOC species and thus have the largest impact (Fig. S5).

As anticipated from the updated gas-phase chemistry for isoprene and terpenes outlined in Schwantes et al. (2020), switching to the MOZART-TS2 chemical mechanism increases surface HCHO and CO concentrations across the CONUS by 3.9-12% (0.1-1.0 ppb) and 0.4-3.5% (0.4-5.7 ppb), respectively. O_3 changes are small but exhibit greater spatial heterogeneity than HCHO and CO, with slight increases in the Midwest, Southwest, and Northeast by 0.8-1.7% on average and decreases on the West Coast, Mountain, and Southeast by 0.5-1.7%, all under 0.8 ppb.

Text S2. Sensitivity to Nudging Strength

Nudging is a modeling technique that involves applying an artificial Newtonian relaxation term based on the difference between the model reference state and meteorological re-analysis data, aiming to improve the agreement between simulated and actual states (Li et al., 2022; Otte, 2008). Stronger nudging of temperature and winds aims to closely replicate real-world meteorological conditions, thereby reducing meteorological bias relative to observations in the model (Davis et al., 2022; Gaubert et al., 2020; Schwantes et al., 2022). However, overly strong nudging can induce artificial mixing of atmospheric tracers, particularly across sharp gradients like those at the tropopause (van Noije et al., 2004). Concerns persist that specified dynamics schemes with nudging may inaccurately represent circulation trends and introduce tracer transport errors (Davis et al., 2022). We thus evaluate the impact of nudging strength by comparing 12-hour and 6-hour relaxation times applied to 'T' (air temperature), 'U' (zonal wind velocity), and 'V' (meridional wind velocity) through two additional simulations (*CAMS_6HrNudge_chemTS1* and *CAMS_6HrNudge_chemTS2*; Table S1) that replicate the *BASE* and *CAMS_chemTS2* setups but use a shorter 6-hour relaxation time (stronger nudging strength).

When comparing simulations using the same nudging strengths with MOZART-TS2 versus MOZART-TS1, we find almost identical responses in the nudged variables T, U, V, and air pollutant concentrations as expected (Fig. S3). Surface conditions are highly

consistent across simulations using the same nudging strength (either 12-hour or 6-hour), with differences typically less than 0.01% for nudged variables and less than 1 ppb for surface O_3 and NO_2, largely driven by meteorological factors such as cloud cover and photolysis rates (see Schwantes et al. 2022 for more on nudging and specified dynamics relaxation times). Notably, the impact of this weather noise is not homogeneous, resulting in greater differences in O_3 than NO_2, and particularly pronounced in the Midwest compared to other regions (Fig. S3).

We find that the differences resulting from nudging when two different relaxation time scales are used exceed differences attributed to switching chemical mechanisms when both perturbations use the same nudging strength. Fig. S3 shows disparities between the MOZART-TS1 simulations using 6-hour and 12-hour nudging (*BASE*) are notably larger and exhibit significant regional variation, even for the nudged variables. Specifically, regional mean temperature changes range from -0.5 K in the Midwest to +0.2 K in the West Coast and Southeast. Changes in zonal (U) and meridional (V) wind velocities are less than 0.3 m/s. Additionally, changes in surface NO_2 concentrations are within 0.05 ppb, whereas surface O_3 shows more pronounced responses, particularly in the Southeast, where changes peak at 1.5 ppb while remaining under 0.8 ppb in other regions (Fig. S3).

We emphasize that changes in concentrations due solely to the nudging configuration are non-negligible, and thus sensitivity tests requiring differencing with a base simulation should always be conducted with a consistent and appropriately selected relaxation time. We adopt a consistent 12-hour relaxation time in our MUSICAv0 sensitivity simulations (Tabel 1) to ensure that differences among simulations reflect the intended perturbations rather than noise arising from differences in the nudging configuration.

Text S3. NEI Processing

We first use the WRF Preprocessing System (WPS), developed for the Weather Research and Forecasting (WRF) model, to create a regular latitude/longitude grid at 0.1° × 0.1° over the contiguous United States (CONUS). Next, we employ the epa_anthro_emis pre-processor, developed by NCAR as one of the tools for the Weather Research and Forecasting model coupled with Chemistry (WRF-Chem), to map the NEI 2017 version 2 emissions onto this 0.1° × 0.1° grid. The processor takes Community Multiscale Air Quality

(CMAQ)-ready day-specific hourly emission files and maps them onto a WRF domain. The NEI 2017 version 2 CMAQ files, originally provided by the U.S. EPA, are at a 12 km × 12 km resolution. Detailed documentation of these tools can be found at https://www2.acom.ucar.edu/wrf-chem/wrf-chem-tools-community.

We verified that hourly NEI data are read by MUSICAv0 in UTC time, as required by the model framework, and that the prescribed grid-cell-level diurnal and weekday-weekend variability is preserved when interpreted in local time (Fig. S6). In MUSICAv0, emissions are ingested at the temporal resolution provided in the input files and, where applicable, linearly interpolated between successive time stamps. By explicitly prescribing emissions at monthly, daily, or hourly resolution, the emission values ingested by the model are unambiguous at each time step. This approach differs from frameworks such as the Harmonized Emissions Component (HEMCO) (Keller et al., 2014; Lin et al., 2021), in which sub-daily variability is imposed via temporal scaling of climatological emissions rather than through explicitly time-resolved emission files.

Fig. S6a shows CONUS-wide maps of hourly NO emissions at four representative UTC times on 12 July 2018, with the corresponding local times indicated for each U.S. time zone. Emissions peak during local morning and daytime hours and are lowest at night, with the pattern progressing westward as local time advances, consistent with emissions being read in UTC while preserving the prescribed diurnal variability in each region's local time. Fig. S6b shows city-mean NO emission time series for six cities over a Monday-Sunday period. When plotted in UTC (top sub-panel), the diurnal cycles are shifted among cities, reflecting longitudinal differences; when plotted in local time (bottom sub-panel), the diurnal cycles align across cities, exhibiting consistent daytime peaks and clear weekday-weekend reductions.

Text S4. Reducing Anthropogenic NO_x and VOC Emissions under *NEI_monthly*

We conduct two additional one-month sensitivity simulations under the *NEI_monthly* case to further examine changes in O_3 and its precursors and investigate the photochemical regime of O_3 production using NEI emissions. One simulation applies a 30% reduction in anthropogenic NO emissions (*NEI_monthly_m30anthroNO*), while the other applies a 30% reduction in anthropogenic VOC emissions (*NEI_monthly_m30anthroVOC*)

(Table 1). The VOC species considered in the latter simulation include acetylene, ethene, ethanol, ethane, propene, propane, methanol, acetone, methyl ethyl ketone (MEK), benzene, toluene, monoterpenes, isoprene, formaldehyde, other aldehydes, alkenes, and alkynes. These simulations specifically provide a comparison to the more nuanced changes resulting from imposing different temporal resolution of anthropogenic emissions in *NEI_hourly*, *NEI_hourly_NO,* and *NEI_daily_NO* simulations.

A 30% reduction in anthropogenic NO emissions results in regional average decreases in surface concentrations of NO (13-21%, 0.02-0.04 ppb), NO_2 (14-21%, 0.1-0.3 ppb), HCHO (2.8-4.5%, 0.1-0.2 ppb), and O_3 (4.7-8.0%, 1.9-2.9 ppb) across all regions (Fig. 3a). Changes in VOC concentrations are minimal (generally less than a 5% increase), except for isoprene, which shows regional mean increases of 7-43% (0.1-0.4 ppb), with the largest changes in VOCs occurring in the Southwest and Southeast. This increase in isoprene is likely driven by reduced OH availability following NO emission reductions, which slows isoprene oxidation by limiting OH regeneration through the NO + HO_2 reaction. Additionally, lower O_3 levels reduce ozonolysis of isoprene and other VOCs as well as OH, further contributing to isoprene accumulation.

A 30% reduction in anthropogenic VOC emissions results in regional average decreases in VOC species primarily from anthropogenic sources, such as benzene (7.7-21%, around 0.01 ppb). In contrast, HCHO and isoprene, which are largely dominated by biogenic sources, show minimal changes: HCHO decreases slightly (0.4-0.7%, 0.01-0.03 ppb), while isoprene exhibits small regional increases of less than 2% in the Northeast, Southwest, and Southeast, and less than 0.2% in other regions. Changes in NO, NO_2 and O_3 are all negligible (less than 0.5% or 0.01 ppb; not shown).

The spatial variations in O_3 concentrations in response to changes in anthropogenic NO or VOC emissions reflect distinct photochemical conditions (Fig. 3a). Metropolitan areas such as New York City (NY) and Los Angeles (CA), which have the highest initial NO emissions relative to their surrounding rural grid cells (Fig. 1), show the largest NO_2 reductions under a 30% decrease in anthropogenic NO emissions (Fig. 4), imply NO_x-saturated regimes since O_3 increases when NO_x levels decrease and O_3 decreases with reductions in VOCs. Conversely, regions outside major cities appear more NO_x-sensitive, where O_3 decreases with reduced NO_x and remains relatively unchanged with VOC

reductions. Overall, O_3 concentrations respond more strongly to a 30% reduction in NO emissions than to an equivalent reduction in anthropogenic VOC emissions.

Text S5. Evaluation of Surface SO_2 and $PM_{2.5}$ Simulations

For the *BASE* simulation, we consistently find a high model bias in surface SO_2, ranging from 50% to 94% (0.9-11 ppb), with poor spatial correlation and high RMSE relative to observations (Table S3). Simulated surface $PM_{2.5}$ exhibits low biases of 15%-44% (1.0-2.4 μg/m^3) in the Mountain, Midwest, and Southwest regions, but is biased high by 27%-34% (3.2-5.1 μg/m^3) in the West Coast, Northeast, and Southeast, with model-observation correlation coefficients varying between 0.15 and 0.75.

Switching to the NEI emissions decreases regional July averages for surface SO_2 and $PM_{2.5}$ by 250-830% (0.3-1.7 ppb) and 2.2-11% (0.3-0.8 μg/m^3), respectively (Fig. S2b). Nevertheless, comparisons with SLAMS observations reveal inconsistent model performance for SO_2 and $PM_{2.5}$, with only some regions improving (Table S3). For SO_2, biases shift from overestimates to underestimates in all regions except the Southwest, with MBE and RMSE values moving closer to zero. However, r_s decreases in the Southwest, Northeast, and Southeast. Spatial correlation for $PM_{2.5}$ improves solely in the Southeast but weakens elsewhere. After incorporating hourly-resolved emissions, we find a regional average increase in monthly mean surface SO_2, ranging from 5-72% (less than 0.1 ppb) and r_s remains low. For surface $PM_{2.5}$, the differences in regional average monthly mean concentrations between *NEI_hourly* and *NEI_monthly* generally increase across the CONUS, ranging from 1.3-11% (0.2-0.7 μg/m^3) (Fig. S2 and Table S3).

Text S6. Evaluation of Emission Timing-Representation Biases in Inferred NO Emissions

We use model simulations to evaluate the timing-representation bias associated with neglecting diurnal variability in anthropogenic NO emissions inferred from polar-orbiting satellite retrievals. This bias is assessed using the *NEI_hourly_NO* (NO emissions varying at hourly resolution following the NEI temporal profile) and *NEI_monthly* (constant emissions) simulations (Table 1), with differences in simulated vertical column densities attributable solely to the temporal allocation of NO emissions. Throughout this section, Ω

denotes the tropospheric NO_2 vertical column density and E denotes anthropogenic NO emissions. All diagnostics are evaluated for July 2018. We define $\Omega'_{\mathrm{obs}} \equiv \Omega_{NEI\_hourly\_NO}$ as a proxy for the "observed" column based on satellite retrievals when emission timing is correctly represented, and $\Omega_M \equiv \Omega_{NEI\_monthly}$ as the "modeled" column used in an emission estimation framework that neglects diurnal emission variability.

As a simple illustration of the potential error in inferred emissions, we follow the mass-balance scaling framework previously used to infer emissions from satellite products (Eq. 2 of Lamsal et al., 2014), in which the emission magnitude inferred for each model grid cell from remotely sensed $\boldsymbol{\Omega}$ can be expressed as

$$\boldsymbol{E_{\mathrm{est}} = E_M \frac{\Omega'_{\mathrm{obs}}}{\Omega_M}},$$

where $\boldsymbol{E_M}$is the *a priori* anthropogenic monthly mean NO emission magnitude used by the model. The resulting fractional bias in inferred emissions attributable solely to unresolved emission timing is therefore

$$\boldsymbol{\left(\frac{\Delta E}{E}\right)_{\mathrm{timing}} = \frac{E_{\mathrm{est}} - E_M}{E_M} = \frac{\Omega'_{\mathrm{obs}}}{\Omega_M} - 1}.$$

Positive values indicate overestimation of emissions, while negative values indicate underestimation. Regional averages are computed as area-weighted means using grid-cell area, and city-scale diagnostics are extracted directly from the corresponding grid-cell indices.

These analyses are intended as transparent, simple diagnostics rather than full inverse modeling exercises. This approach assumes that anthropogenic NO emissions are injected near the surface within the planetary boundary layer and that, in polluted regions, $\boldsymbol{\Omega}$ at the satellite overpass time is strongly influenced by boundary-layer NO_2, allowing $\boldsymbol{\Omega}$ to serve as a proxy for surface emissions. It further assumes approximate linearity between fractional changes in emissions and early-afternoon $\boldsymbol{\Omega}$ over the perturbation range considered.

(a)

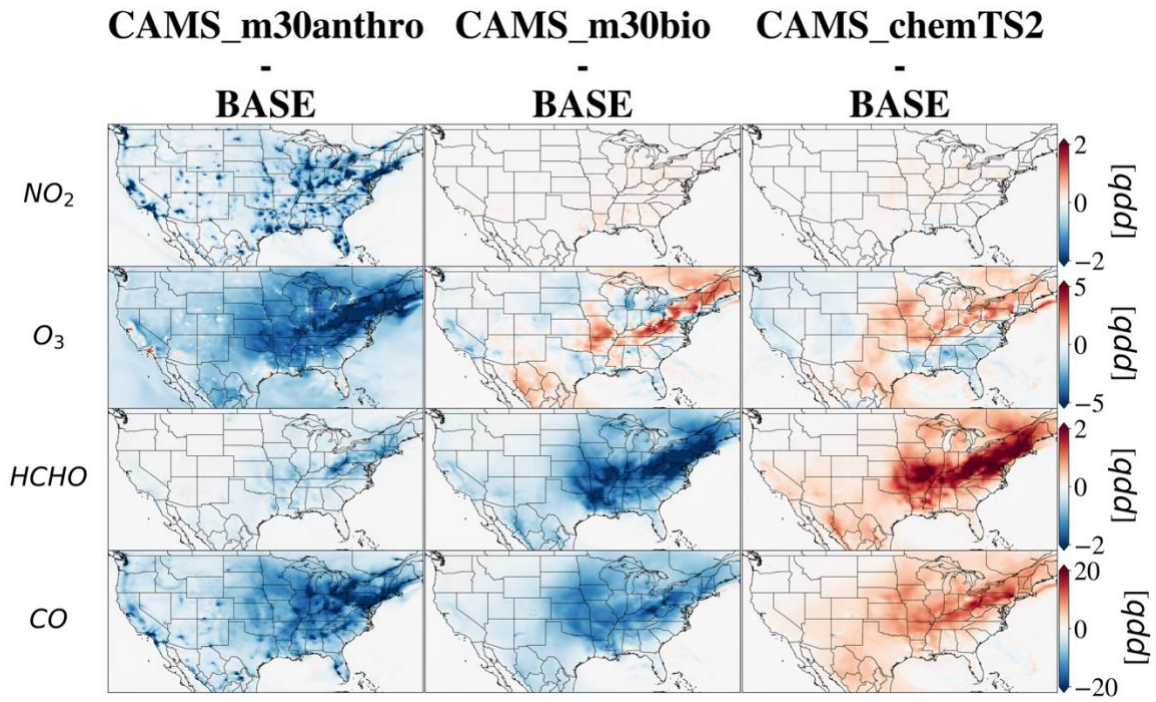
CAMS_m30anthro - BASE
CAMS_m30bio - BASE
CAMS_chemTS2 - BASE
NO2
O3
HCHO
CO
2
0
−2
5
0
−5
2
0
−2
20
0
−20
[ppb]

(b)

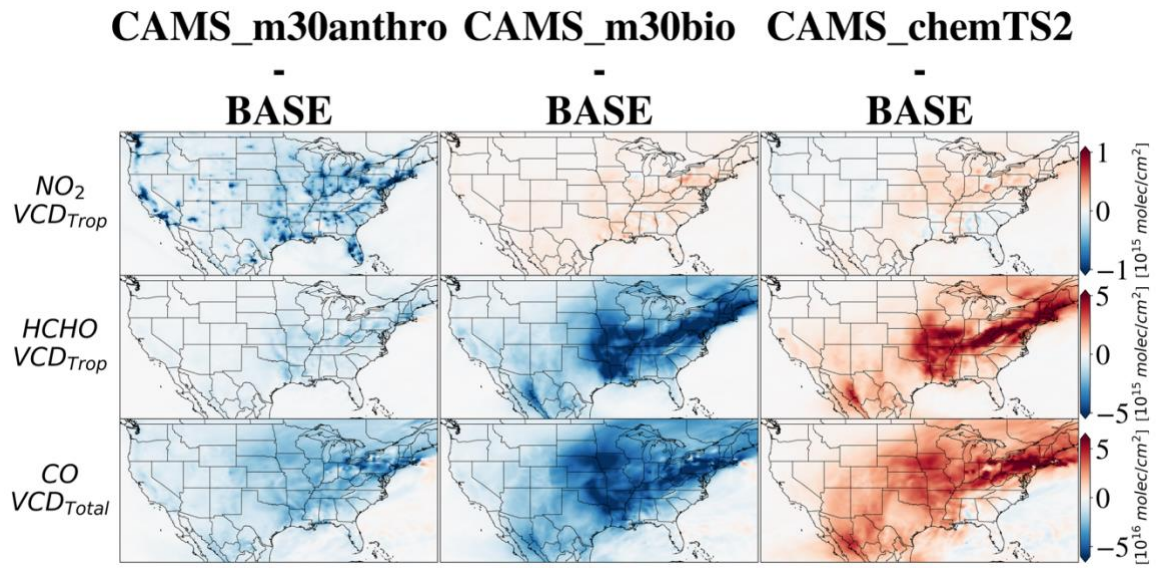
CAMS_m30anthro - BASE
CAMS_m30bio - BASE
CAMS_chemTS2 - BASE
NO2 VCDTrop
HCHO VCDTrop
CO VCDTotal
1
0
−1
5
0
−5
5
0
−5
[10^15 molec/cm^2]
[10^15 molec/cm^2]
[10^16 molec/cm^2]

(c)

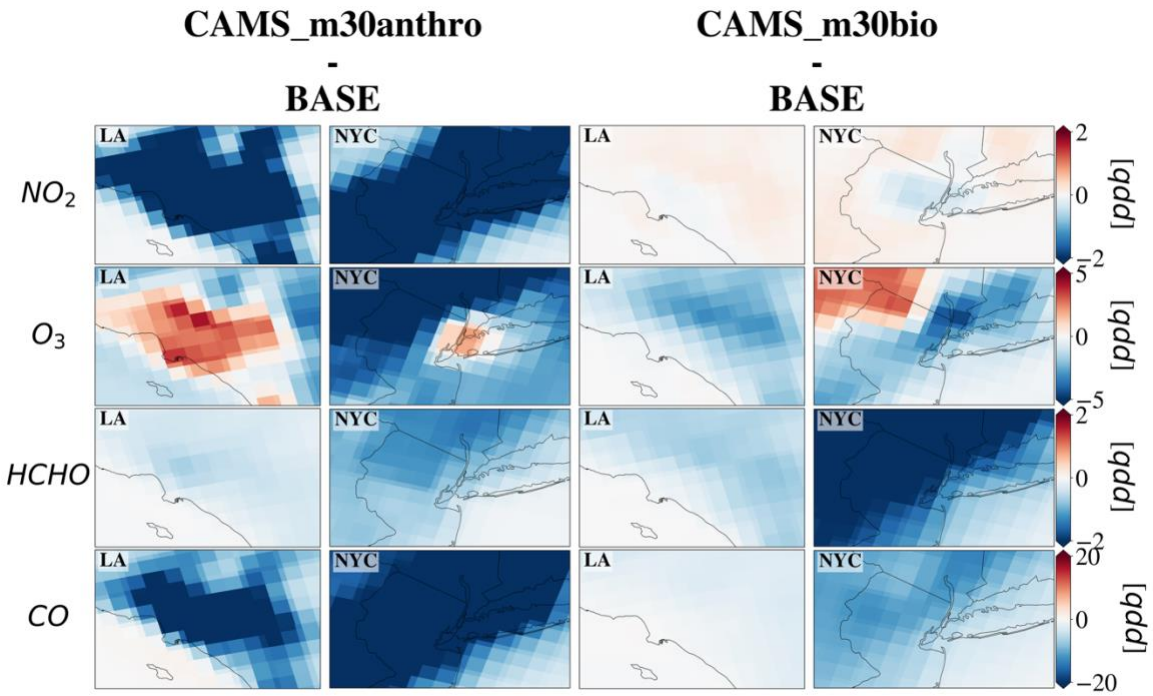

(d)

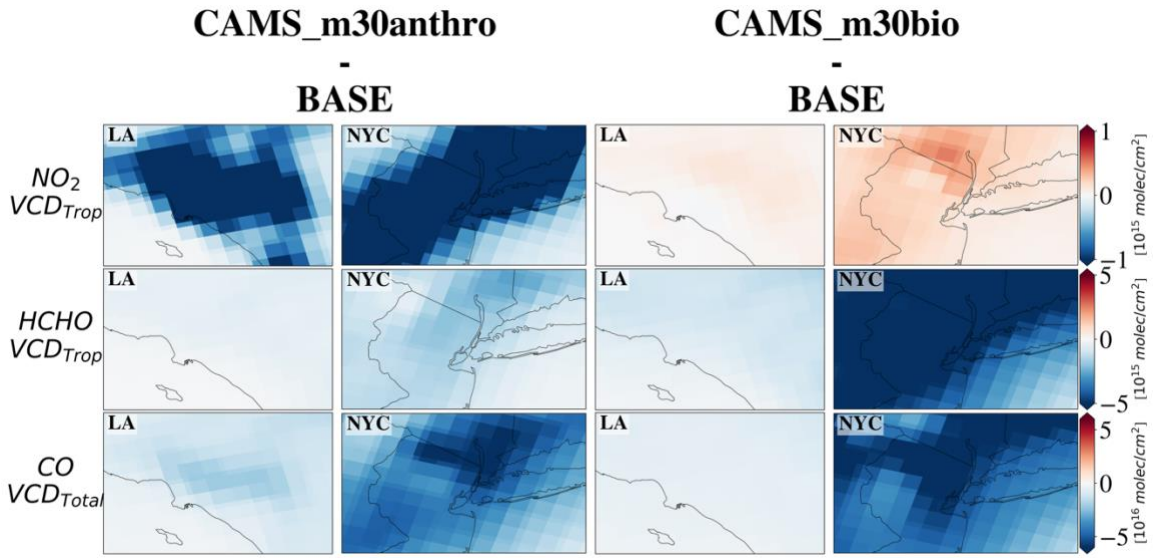

Fig. S1. Responses of selected trace gas species to five-day perturbation simulations (July 1-5, 2018; Table S1), shown as differences in five-day mean surface concentrations (a, c) and column densities (b, d) relative to the *BASE* case. Panels (c, d) are zoomed views of (a, b) over Los Angeles (LA) and New York City (NYC). Consistent color-bar ranges are used for each variable.

(a)

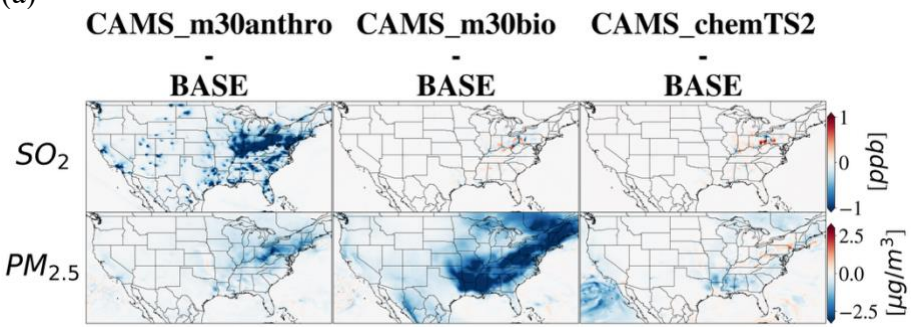

(b)

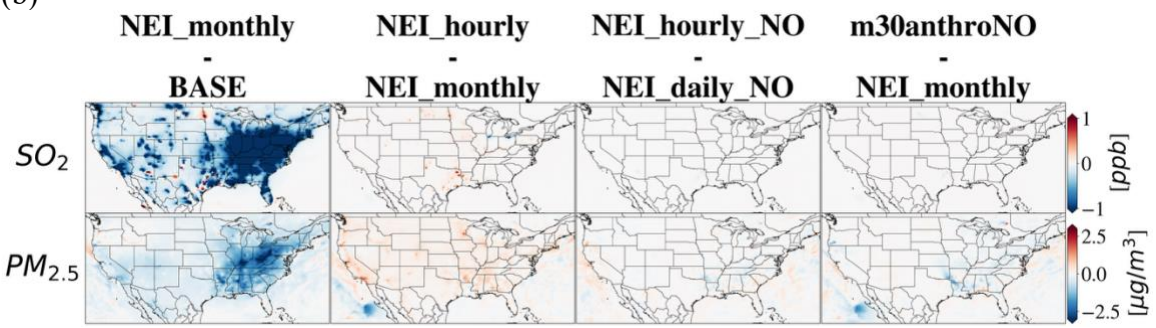

Fig. S2. Panel (a) corresponds to Fig. S1a, and panel (b) corresponds to Fig. 3a, but for changes in surface concentrations of SO_2 (first rows) and $PM_{2.5}$ (second rows).

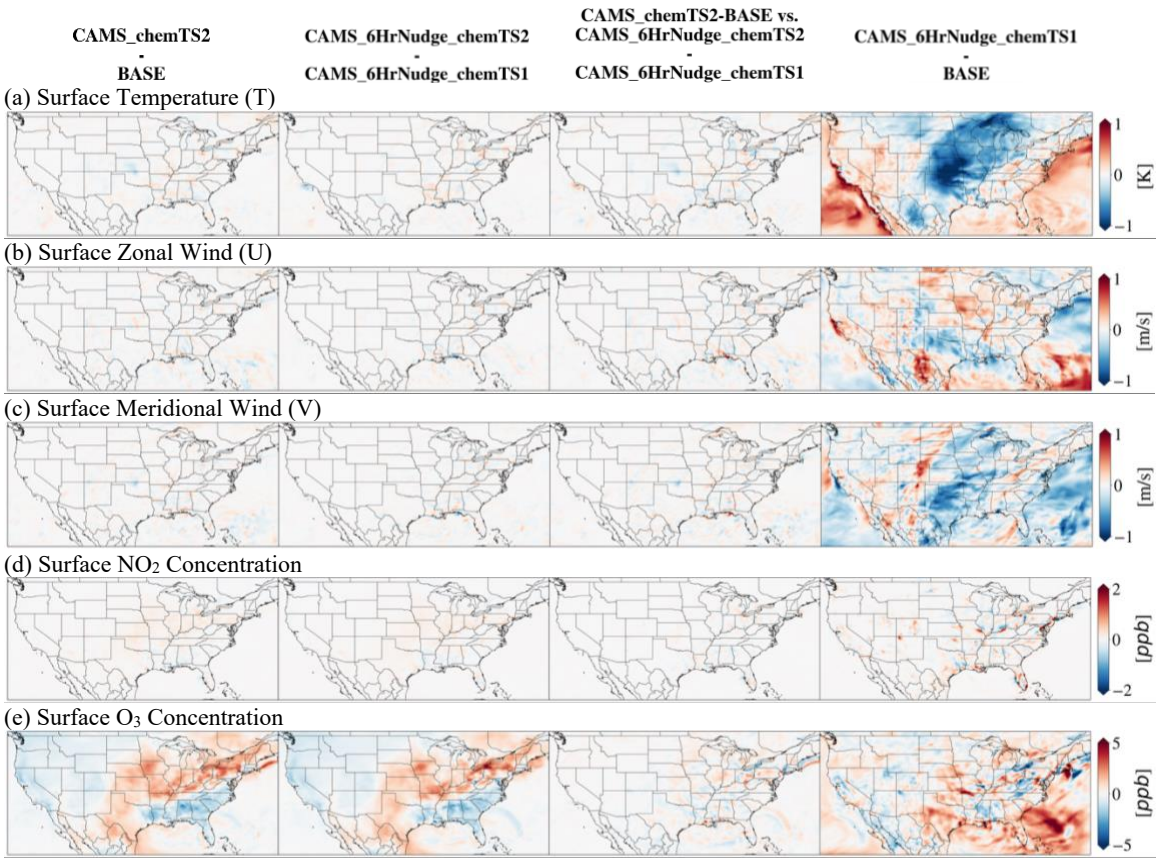

Fig. S3. Differences for surface T, U, V, NO_2 and O_3 concentrations across simulations using the MOZART-TS1 (*BASE*) and MOZART-TS2 chemical mechanisms with 12-hour (*CAMS_chemTS2*) and 6-hour nudging relaxation times (*CAMS_6HrNudge_chemTS1* and *CAMS_6HrNudge_chemTS2*). Simulations using the same nudging strength produce similar meteorological conditions and trace gas concentrations, whereas changing the nudging strength can lead to substantial differences. The first two columns compare MOZART-TS1 versus MOZART-TS2 differences for each nudging option, while the third column contrasts these differences across different nudging options. The rightmost column contrasts the impacts of 6-hour nudging on simulations with the *BASE* 12-hour simulations.

(a) July Mean NEI 2017 Emissions Adjusted for 2018 [kg m^{-2} s^{-1}]

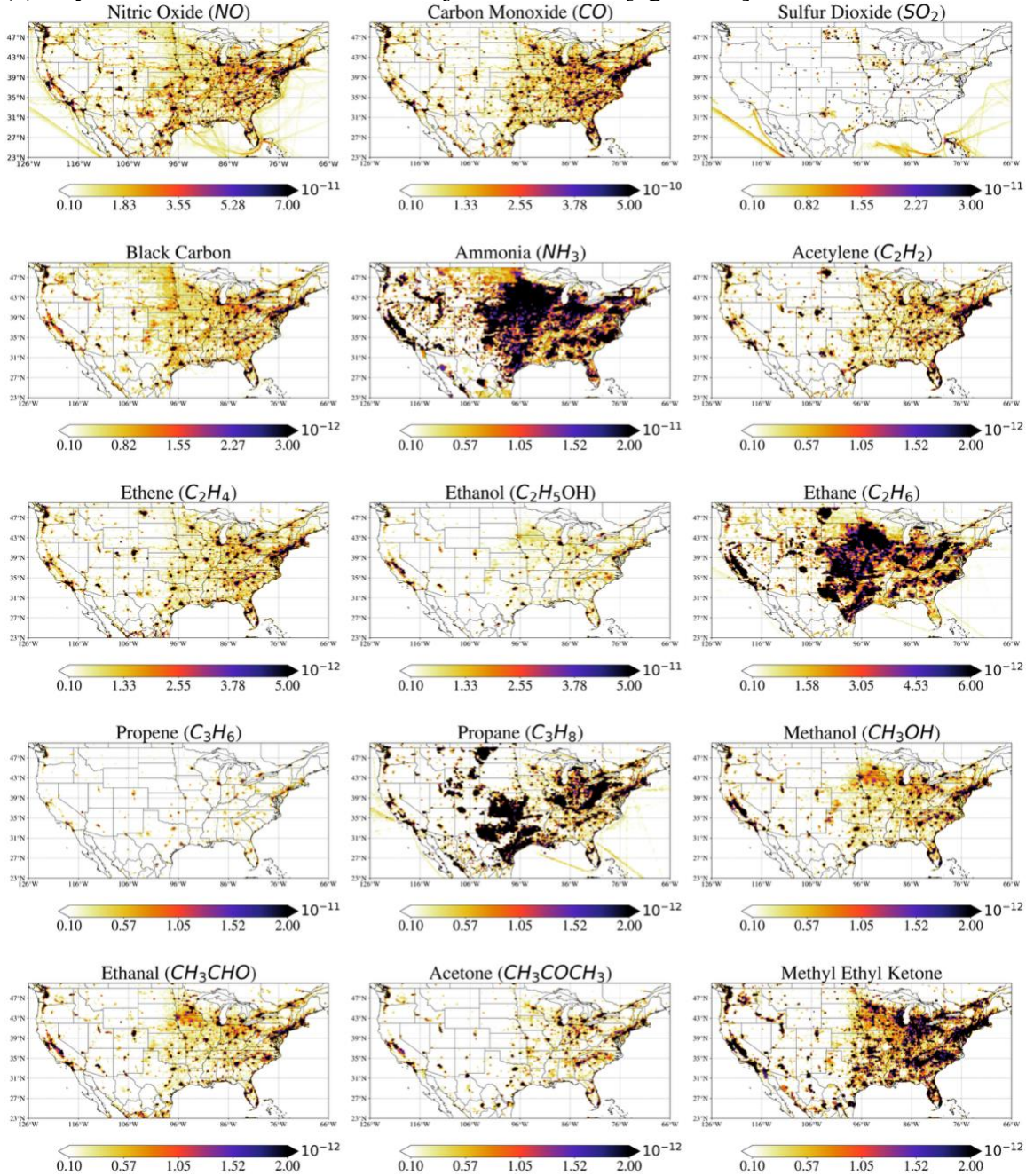

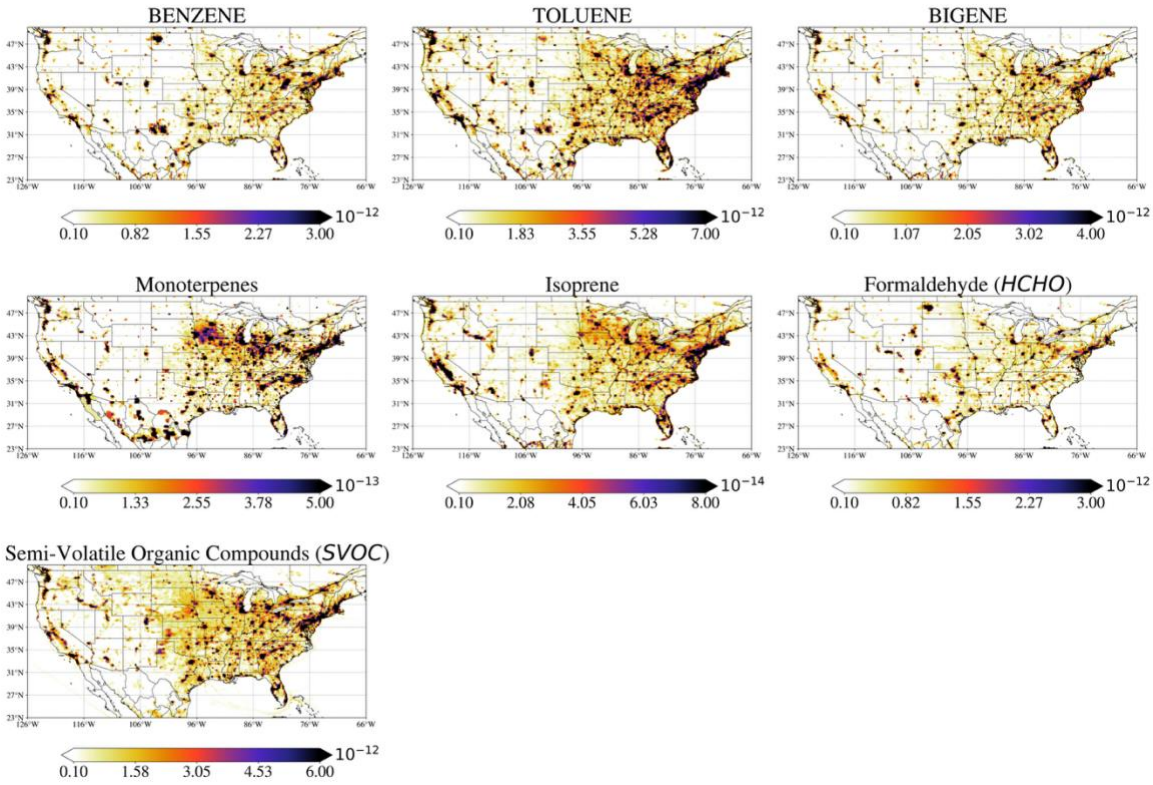
BENZENE
0.10 0.82 1.55 2.27 3.00 10^{-12}
TOLUENE
0.10 1.83 3.55 5.28 7.00 10^{-12}
BIGENE
0.10 1.07 2.05 3.02 4.00 10^{-12}
Monoterpenes
0.10 1.33 2.55 3.78 5.00 10^{-13}
Isoprene
0.10 2.08 4.05 6.03 8.00 10^{-14}
Formaldehyde (HCHO)
0.10 0.82 1.55 2.27 3.00 10^{-12}
Semi-Volatile Organic Compounds (SVOC)
0.10 1.58 3.05 4.53 6.00 10^{-12}

(b) July Mean CAMS-GLOB-ANT v5.1 Emissions [kg m^{-2} s^{-1}]

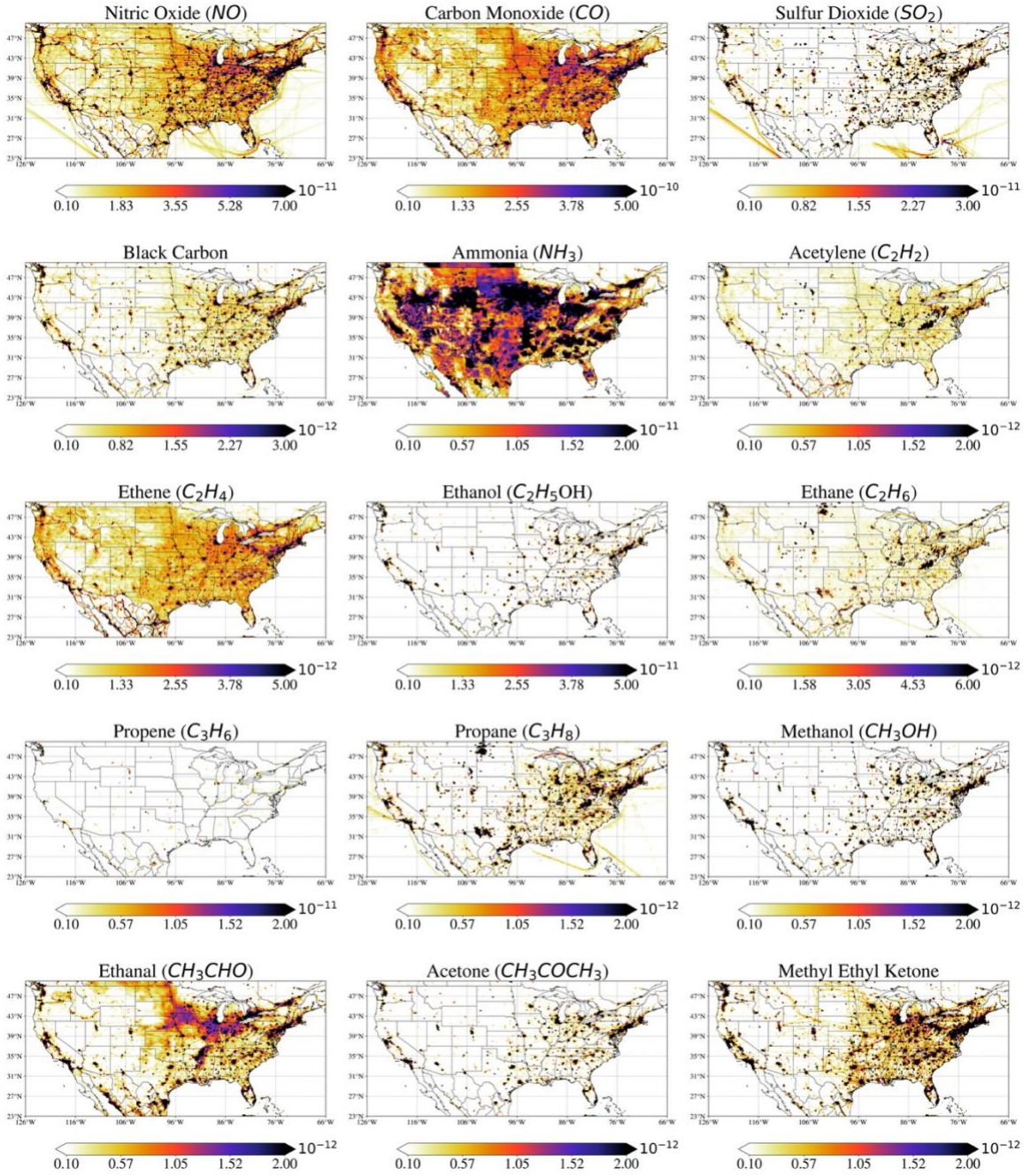

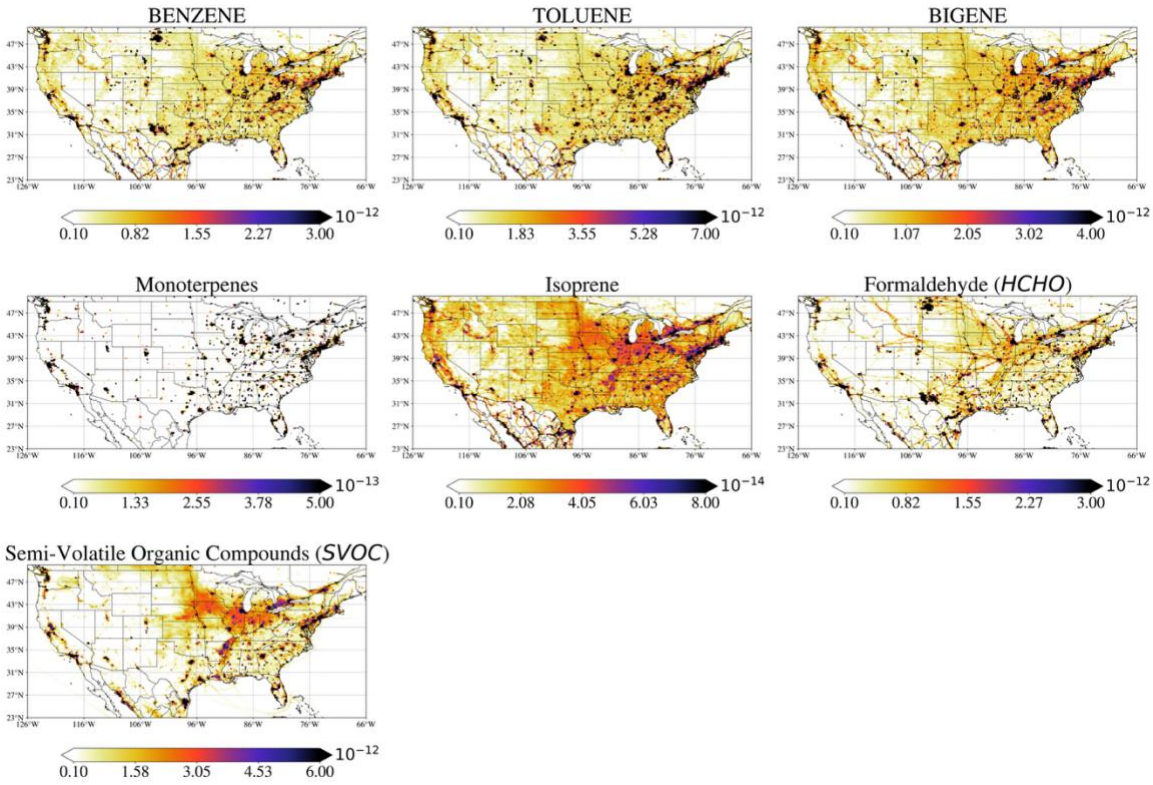
BENZENE
0.10 0.82 1.55 2.27 3.00 10^{-12}
TOLUENE
0.10 1.83 3.55 5.28 7.00 10^{-12}
BIGENE
0.10 1.07 2.05 3.02 4.00 10^{-12}
Monoterpenes
0.10 1.33 2.55 3.78 5.00 10^{-13}
Isoprene
0.10 2.08 4.05 6.03 8.00 10^{-14}
Formaldehyde (HCHO)
0.10 0.82 1.55 2.27 3.00 10^{-12}
Semi-Volatile Organic Compounds (SVOC)
0.10 1.58 3.05 4.53 6.00 10^{-12}

(c) July Mean Adjusted NEI Minus CAMS-GLOB-ANT Emissions [kg m^{-2} s^{-1}]

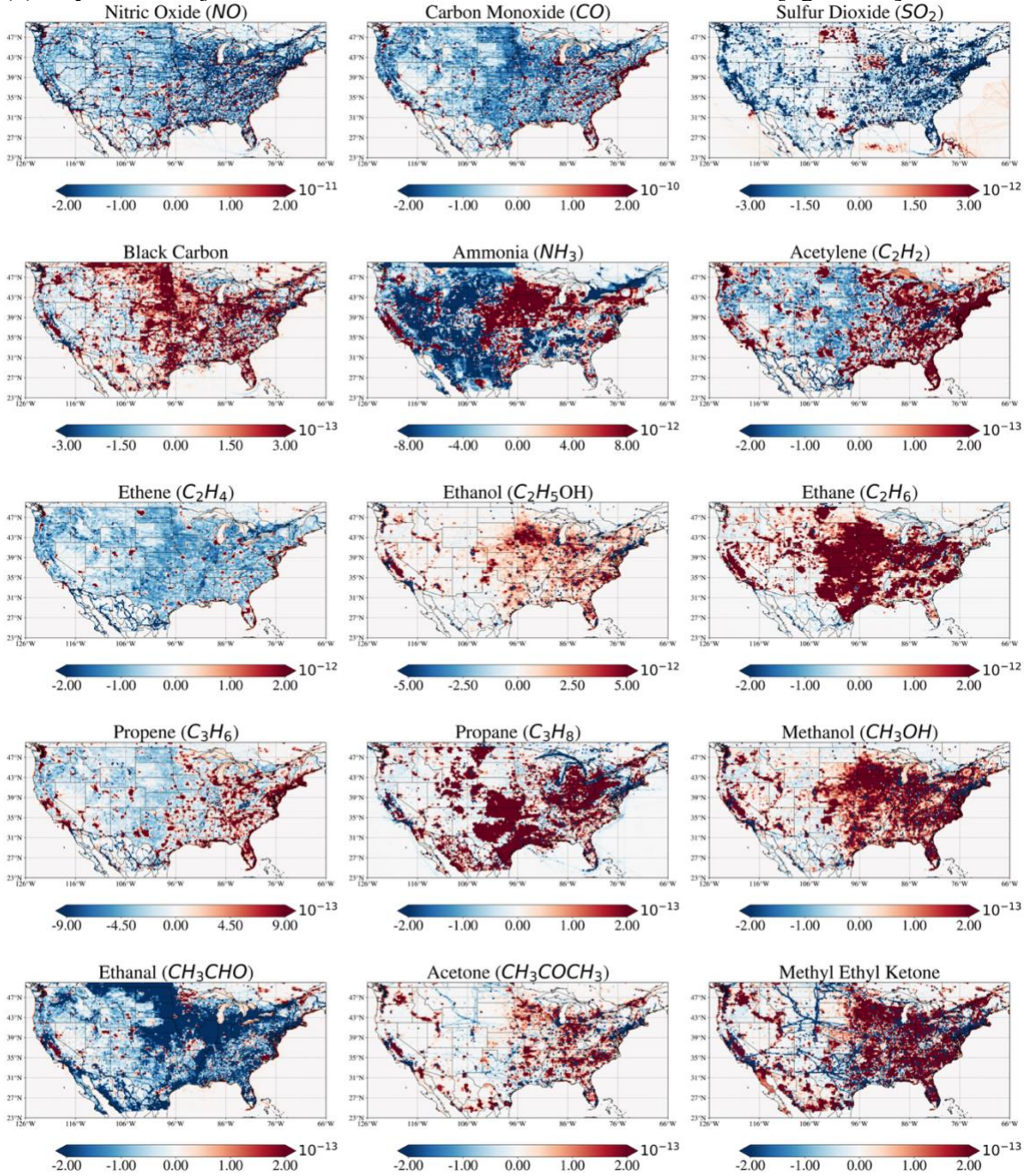

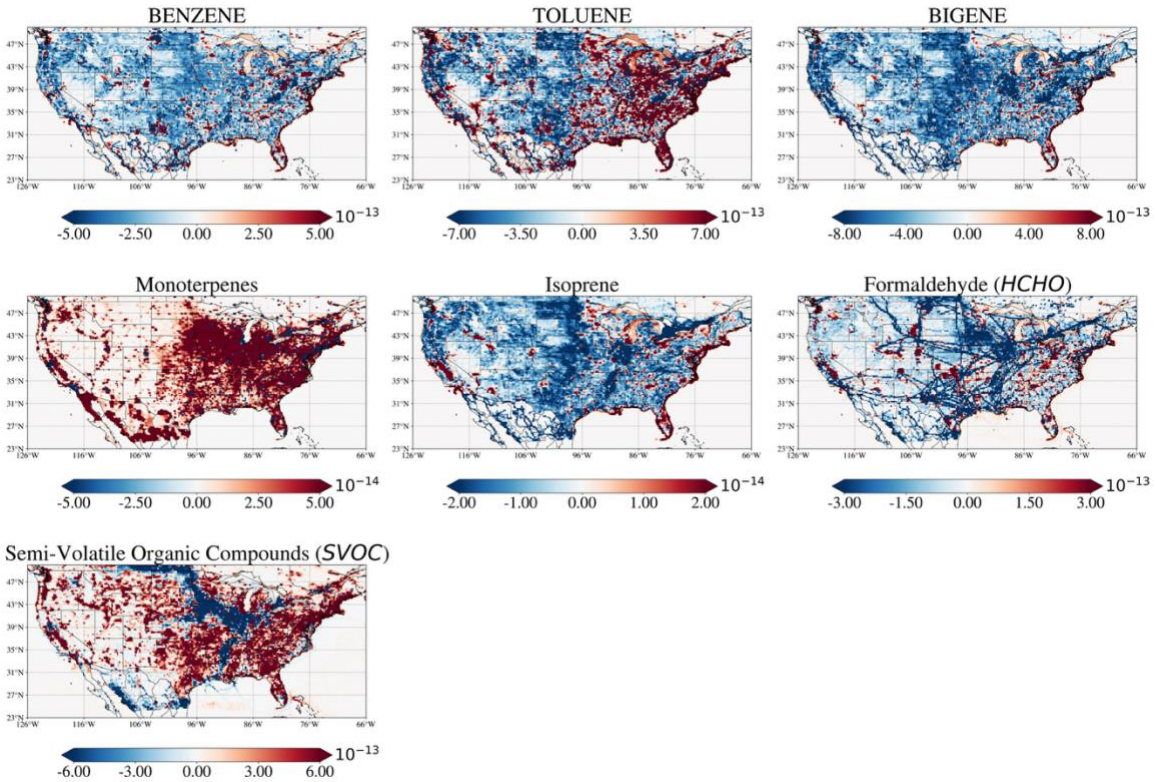

Fig. S4: Spatial distribution of July mean emissions from the adjusted 2017 U.S. National Emissions Inventory (NEI; panel a), Copernicus Atmosphere Monitoring Service (CAMS-GLOB-ANT v5.1; panel b), and their differences (panel c) for each species replaced with NEI emissions in the MUSICAv0 simulations over the contiguous United States (CONUS).

MEGAN Biogenic Emissions [kg m^{-2} s^{-1}]

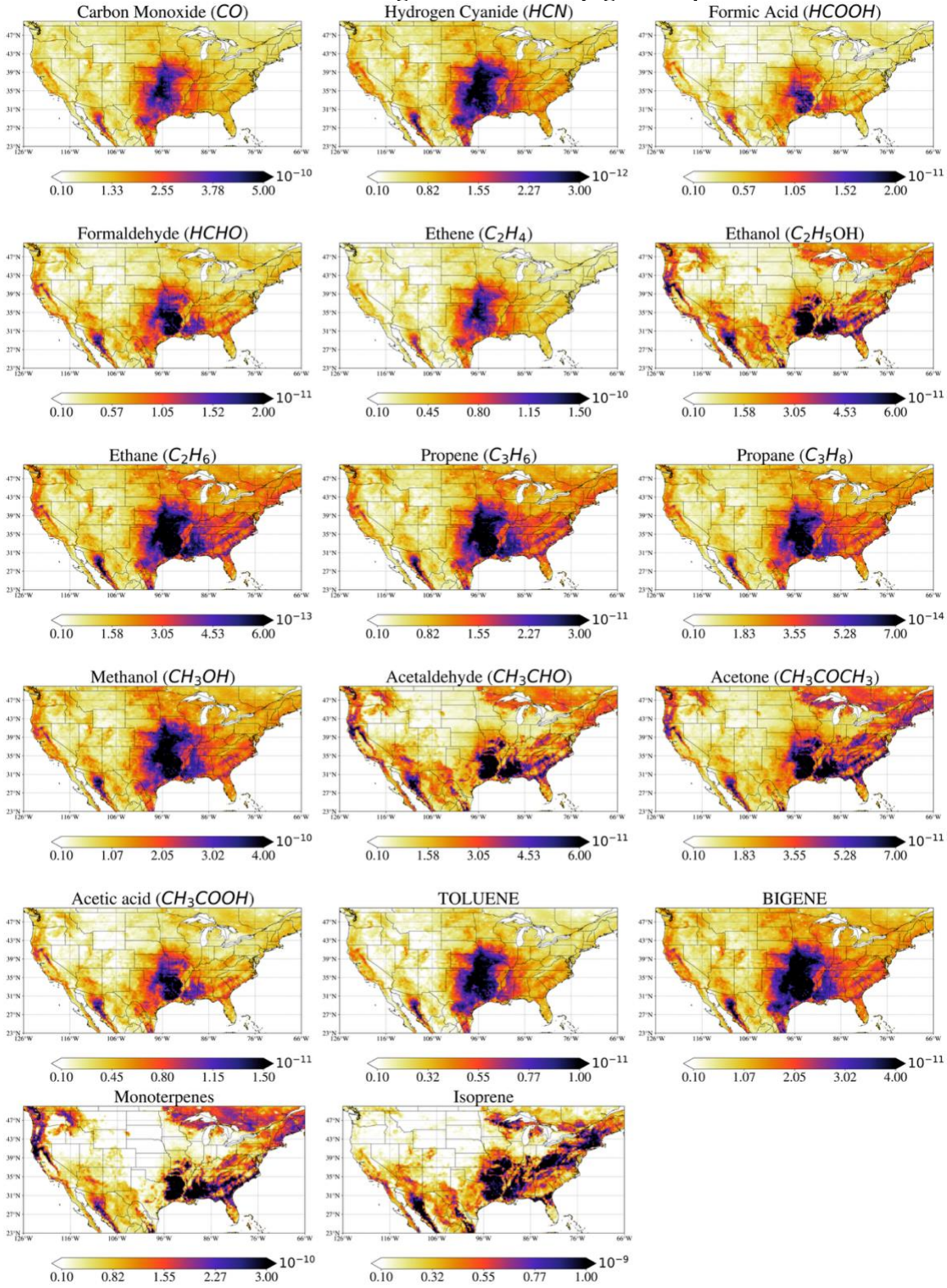

Fig. S5. The spatial distribution of biogenic emissions calculated online in the land component of CESM using the Model of Emissions of Gases and Aerosols from Nature (MEGAN) version 2.1 in the *NEI_monthly* case simulation. Relative differences in any biogenic emission species across the NEI simulations remain below 10%, even in the grid cell with the largest change, which occurs primarily in the southern CONUS due to weather-induced variability that persists even with 12-hour nudging (not shown).

(a)

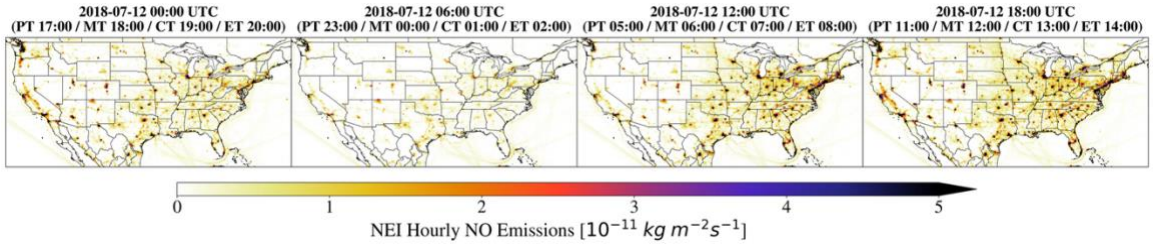

(b)

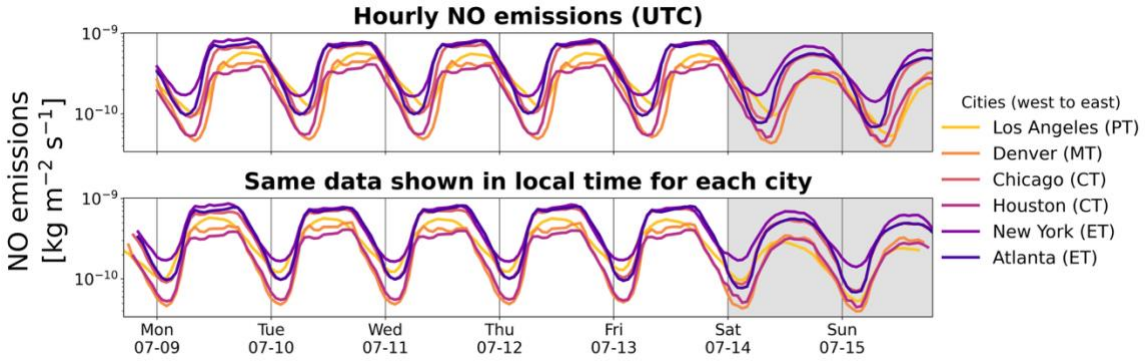

Fig. S6. Diurnal variability in hourly anthropogenic NO emissions from the NEI. (a) Spatial distribution of NO emissions over the CONUS at four UTC times on 12 July 2018 (00, 06, 12, and 18 UTC), with corresponding local times for the Pacific (PT), Mountain (MT), Central (CT), and Eastern (ET) time zones indicated above each panel. (b) Hourly NO emission time series for six representative U.S. cities (Fig. 1; ordered west to east) plotted in UTC (top) and local time (bottom), shown for one grid cell per city during a Monday-Sunday week in July 2018. Weekend days are shaded and the vertical black line marks midnight.

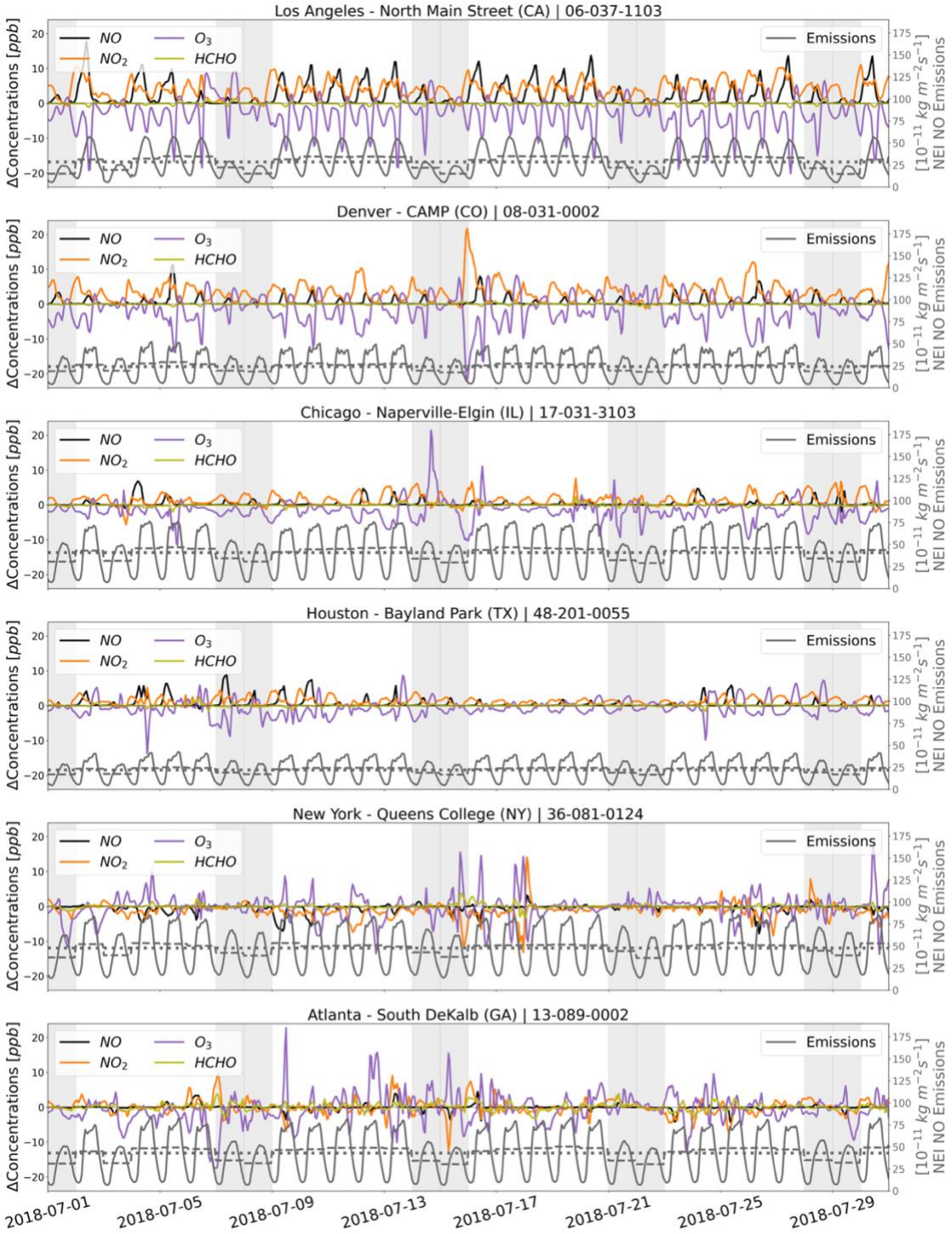

Fig. S7: Hourly time series of July differences in surface NO (black), NO_2 (orange), O_3 (purple), and HCHO (olive) concentrations between *NEI_hourly_NO* and *NEI_daily_NO* simulations, alongside NO emissions represented as hourly values (solid gray), daily means (dashed), and monthly means (dotted). All data are in local time; weekends are shaded in gray.

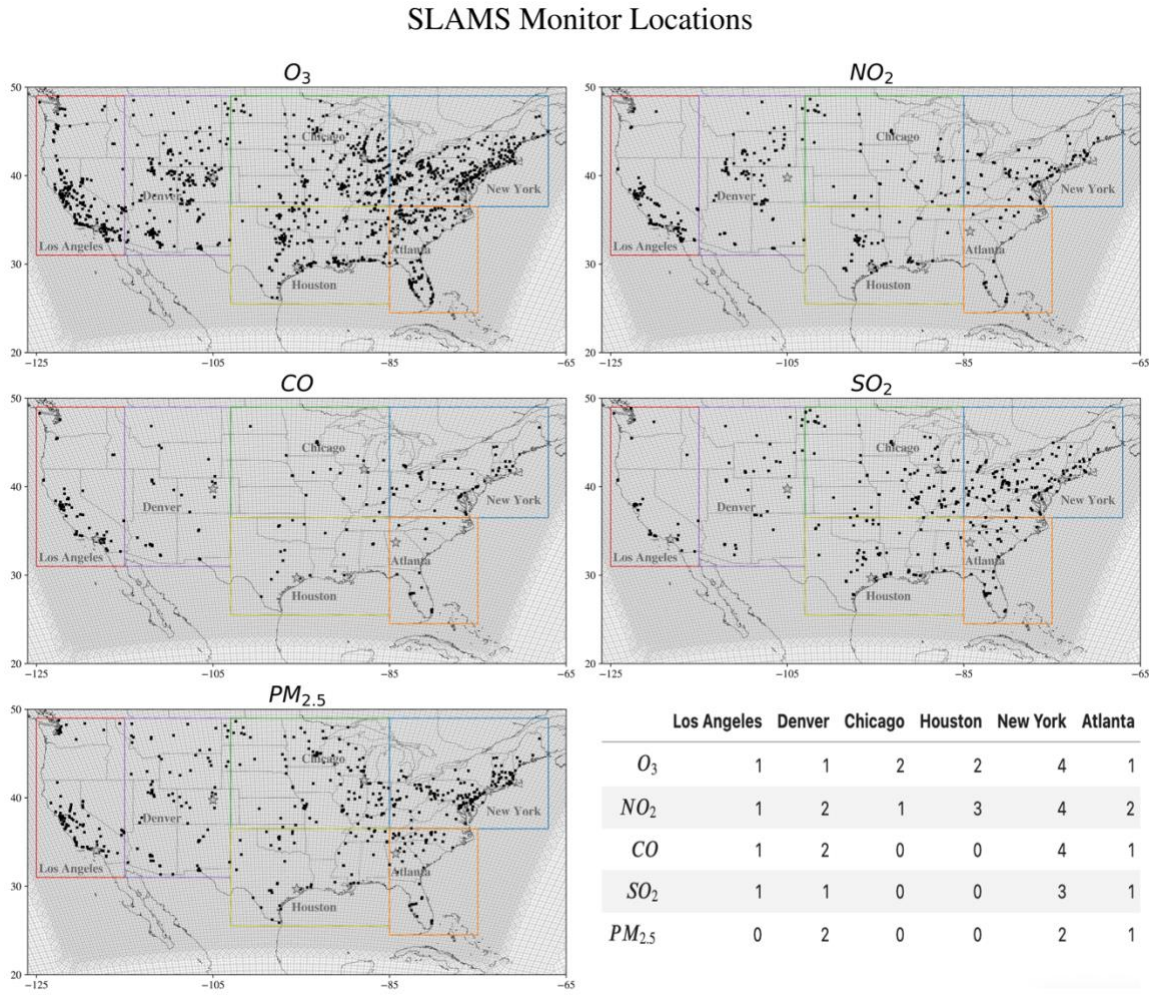

	Los Angeles	Denver	Chicago	Houston	New York	Atlanta
O_3	1	1	2	2	4	1
NO_2	1	2	1	3	4	2
CO	1	2	0	0	4	1
SO_2	1	1	0	0	3	1
$PM_{2.5}$	0	2	0	0	2	1

Fig. S8: Locations of State and Local Air Monitoring Stations (SLAMS) used in this study for surface O_3, NO_2, CO, SO_2, and $PM_{2.5}$. Black squares indicate individual monitoring sites, overlaid on the MUSICAv0 ne0CONUSne30x8 grid (gray lines). Colored boxes denote the six CONUS regions (West Coast, Mountain, Midwest, Southwest, Northeast, and Southeast), and gray stars mark the six example urban cities defined in Fig. 1. The accompanying table summarizes the number of available SLAMS sites per species within the model grid cell containing each city.

(a)

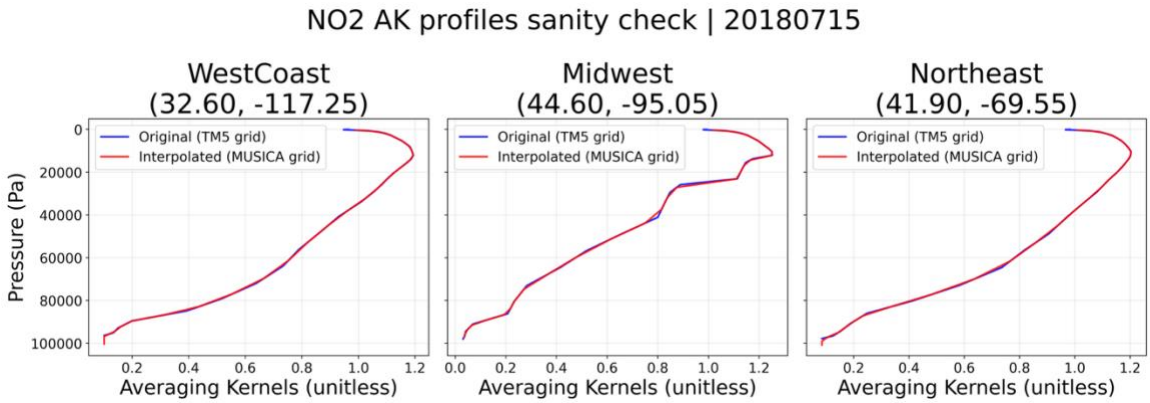

(b)

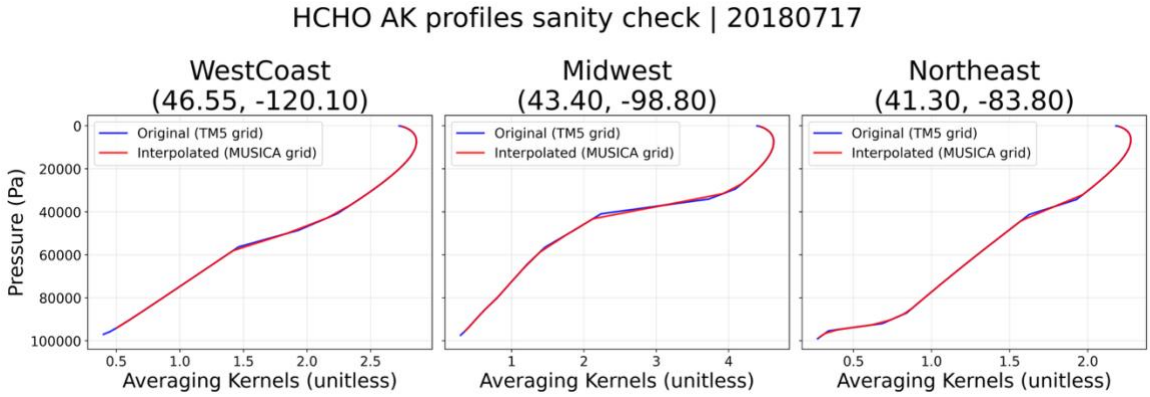

(c)

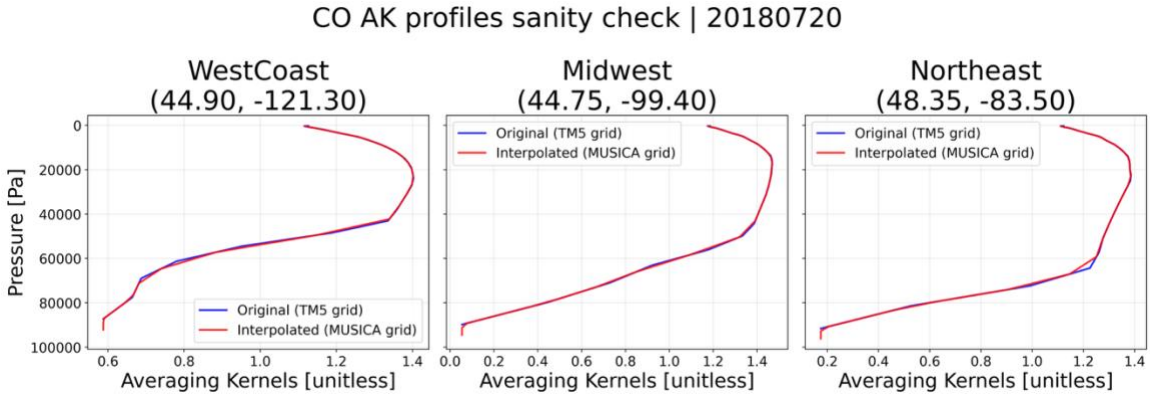

Fig. S9: Comparison of TROPOMI averaging kernel (AK) vertical profiles before and after interpolation from the TM5 grid to the MUSICA grid for NO_2, HCHO, and CO. Original TM5-grid AKs (blue) and interpolated MUSICA-grid AKs (red) are shown for randomly selected pixels and days.

Observed versus Modeled Hourly Concentrations

(a) Surface NO_2

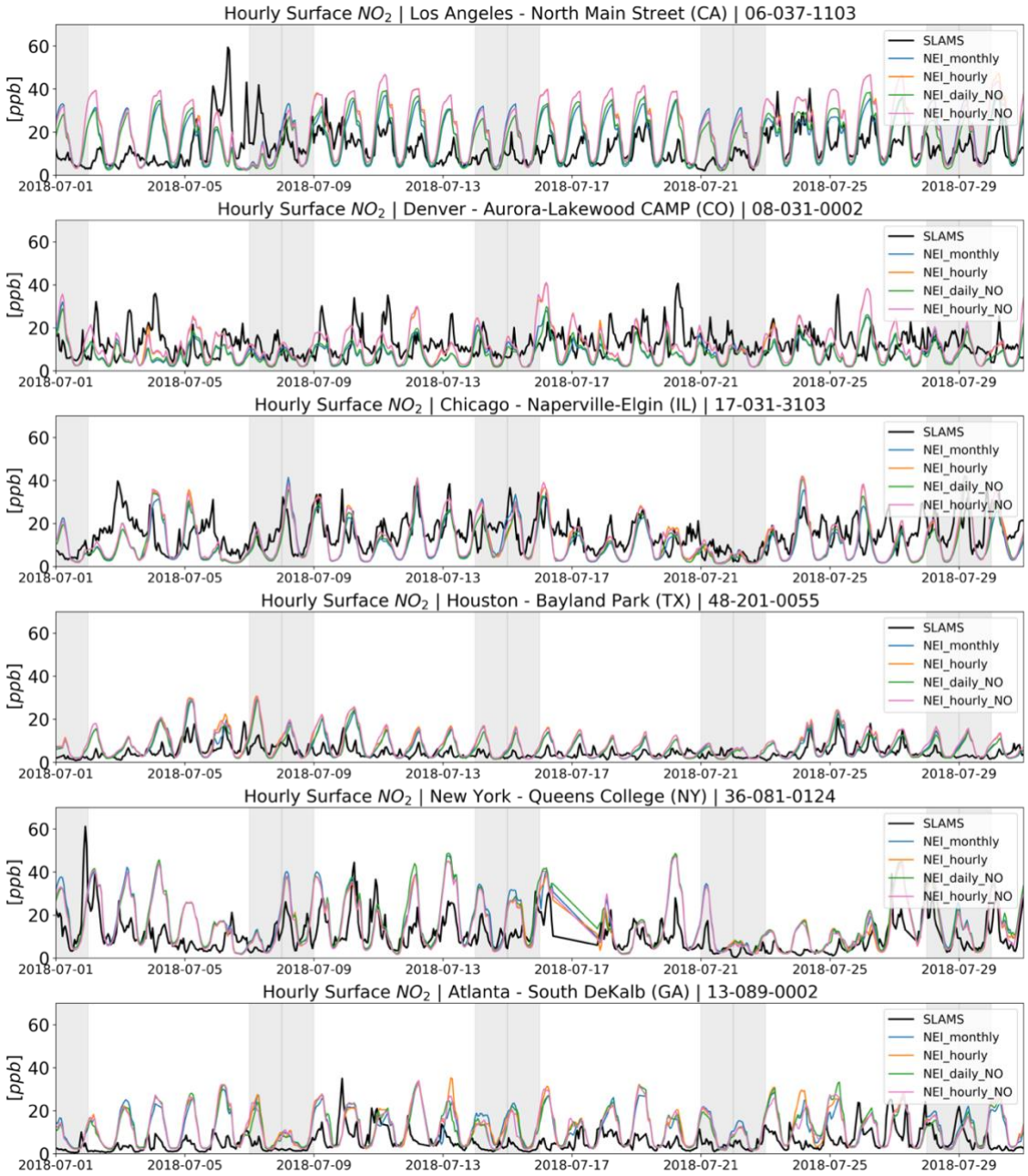

(b) Surface O_3

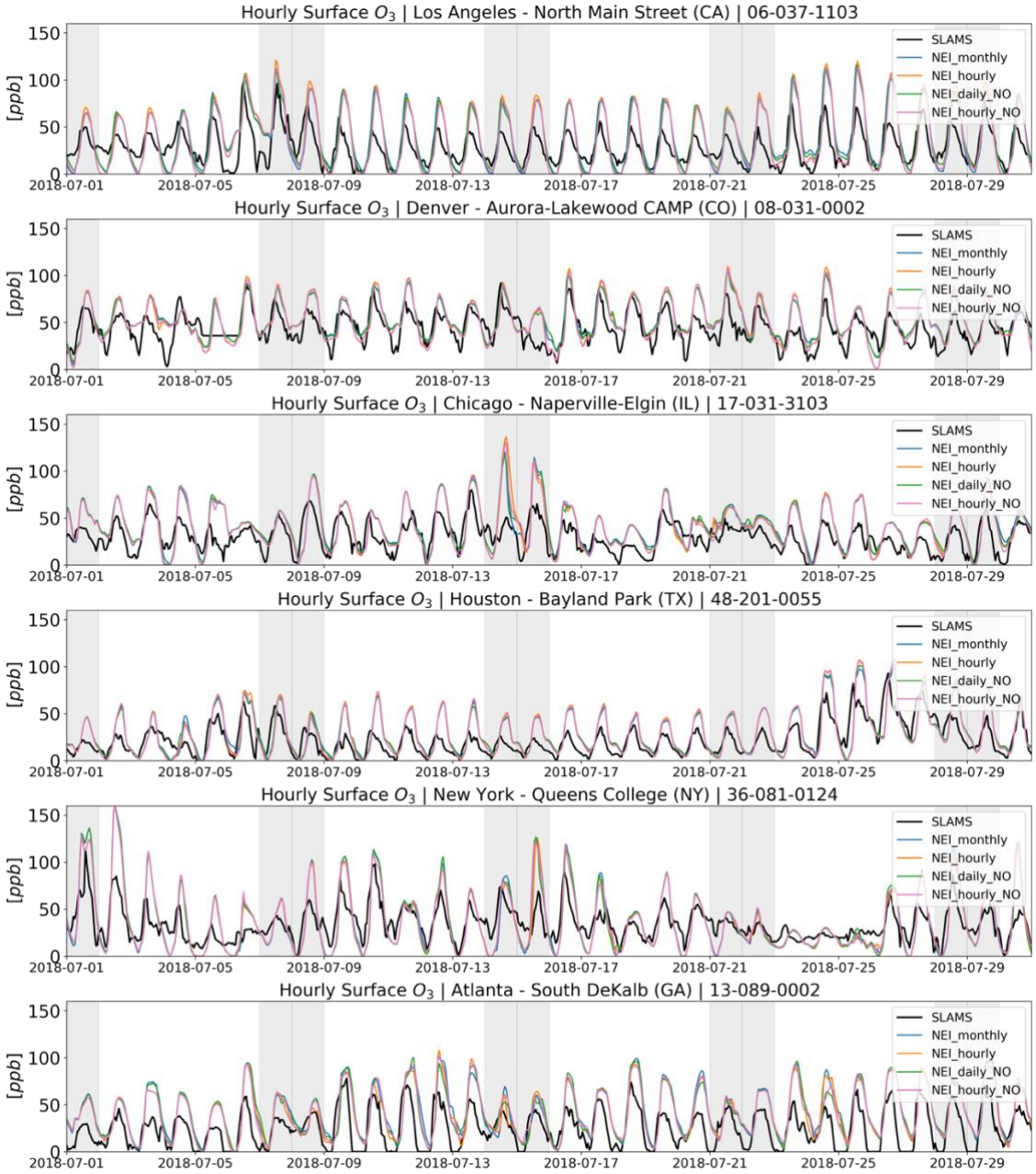

Fig. S10: Hourly variations in surface (a) NO_2 and (b) O_3 concentrations from SLAMS observations (black) and model simulations (colored) for July 2018 at six selected urban monitoring stations (Table S5). Model simulations are shown in four scenarios: *NEI_monthly* (blue), *NEI_hourly* (orange), *NEI_daily_NO* (green), and *NEI_hourly_NO* (pink) (Table 1). Near-surface simulations are approximated at the nearest pixel to each monitoring station. Weekend days (Saturdays and Sundays) are marked in gray.

(a) Surface NO_2

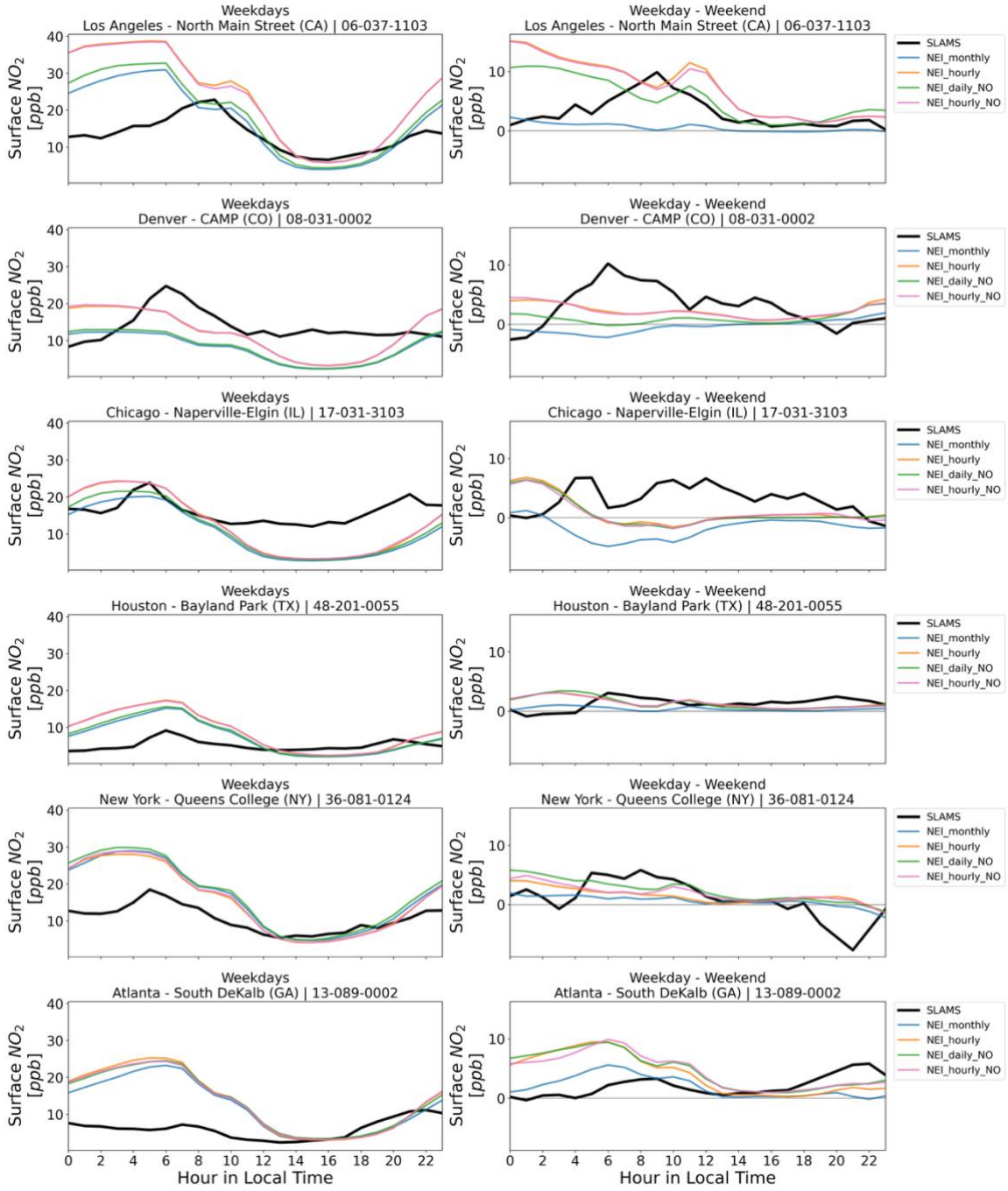

(b) Surface O_3

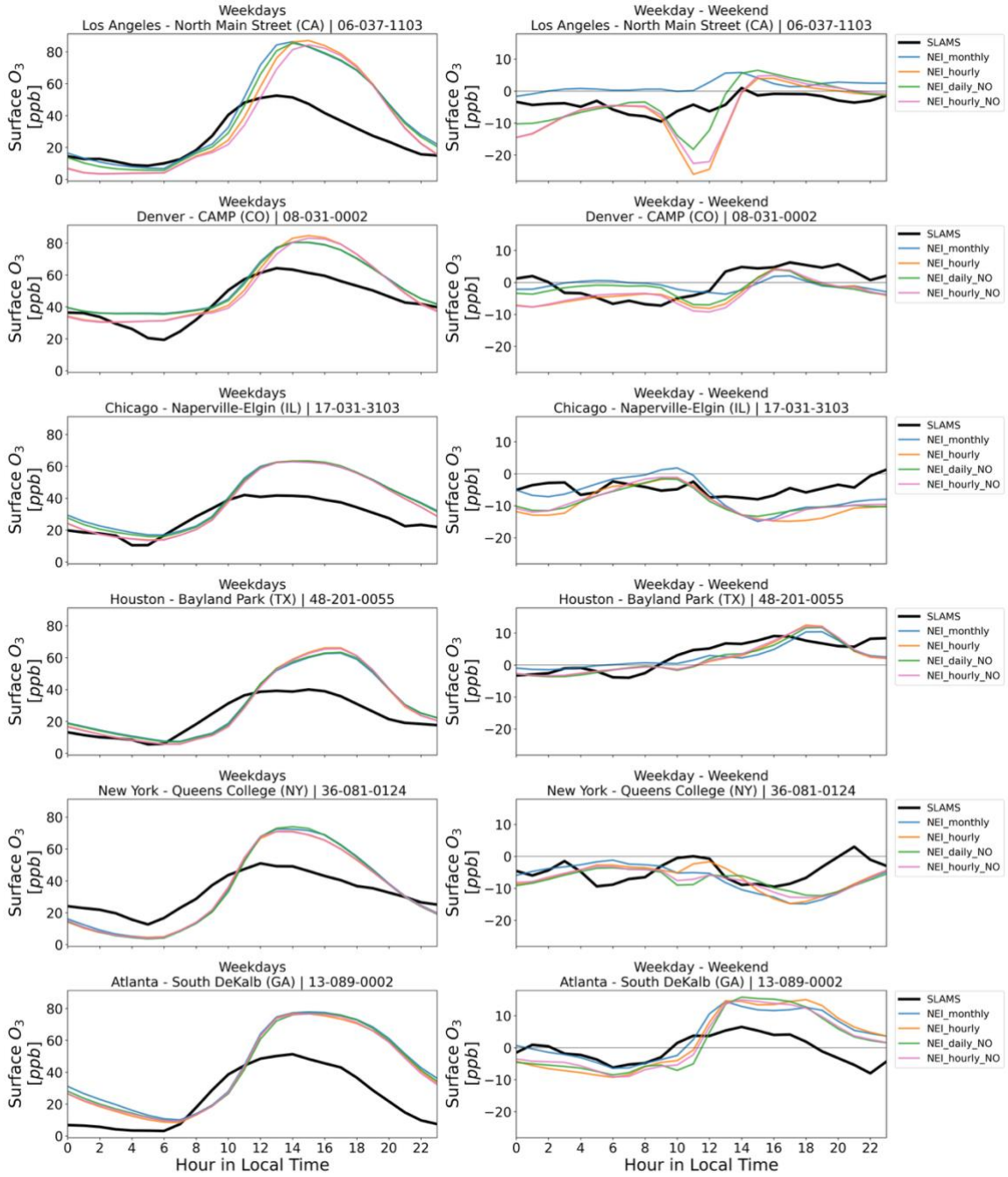

Fig. S11: MUSICAv0 simulated (colored) and observed (black) hourly variations in surface (a) NO_2 and (b) O_3 concentrations averaged for July 2018, for weekdays (left column) and weekday-minus-weekend differences (right column; horizontal gray line indicates zero change) at six urban monitoring stations (Table S5). Model simulations are approximated at the nearest pixel to each monitoring station and shown for four scenarios: *NEI_monthly* (blue), *NEI_hourly* (orange), *NEI_daily_NO* (green), and *NEI_hourly_NO* (pink) (Table 1).

(a) *NEI_hourly_NO – NEI_monthly*

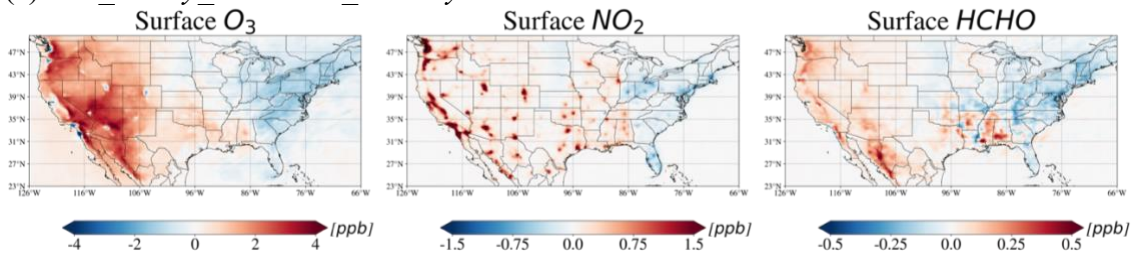

(b) *NEI_daily_NO – NEI_monthly*

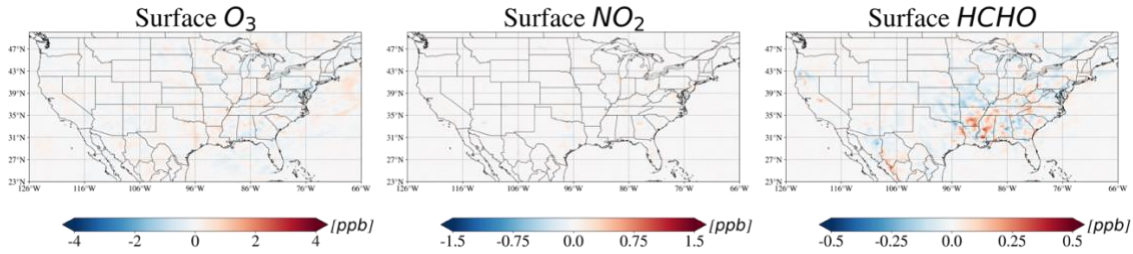

Fig. S12: July mean differences in simulated surface concentrations of O_3, NO_2, and HCHO between (a) *NEI_hourly_NO* and *NEI_monthly*, and (b) *NEI_daily_NO* and *NEI_monthly*. These comparisons complement Fig. 3, highlighting that the spatial differences are primarily driven by the inclusion of hourly variability in NO emissions.

(a)

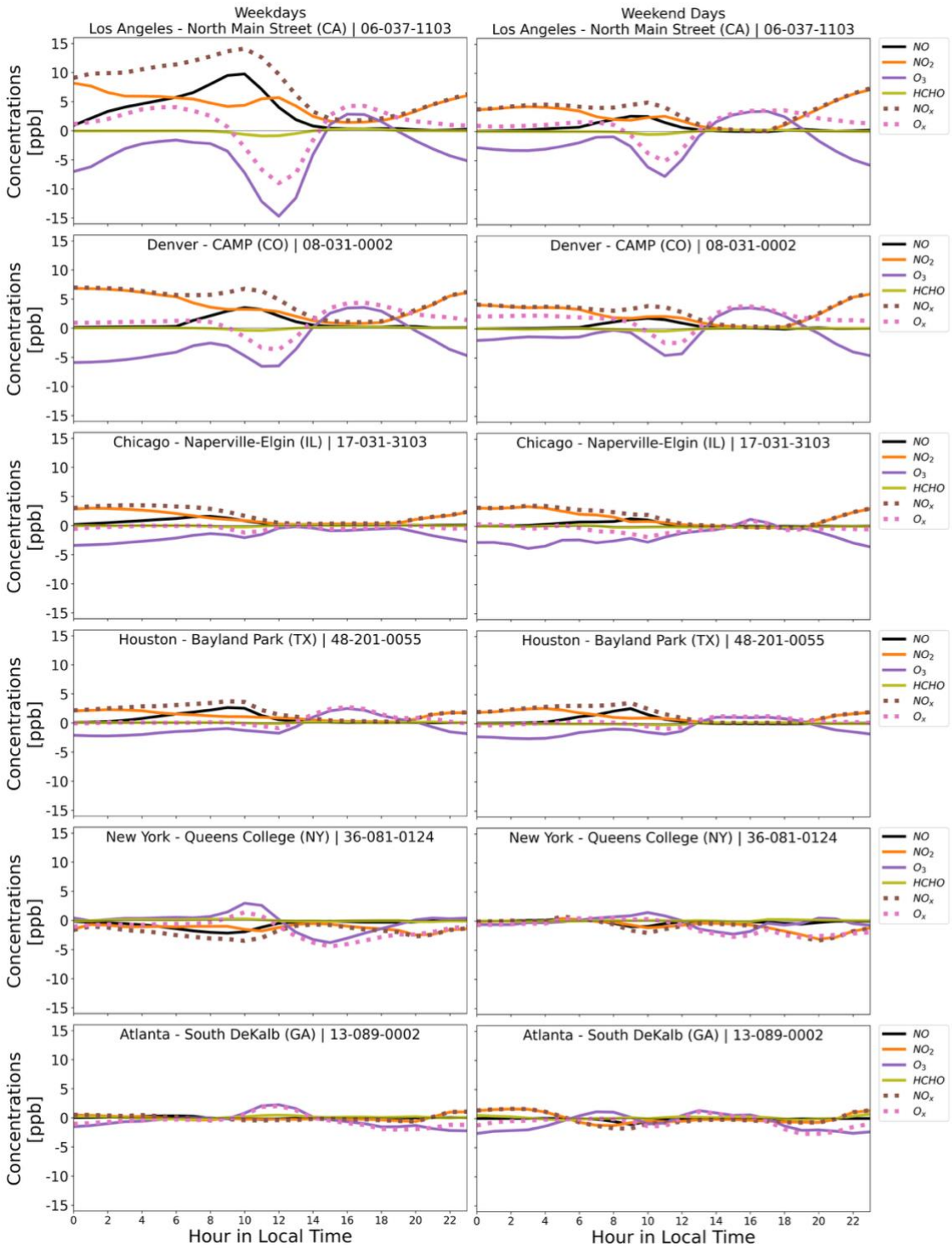
Weekdays
Los Angeles - North Main Street (CA) | 06-037-1103
Weekend Days
Los Angeles - North Main Street (CA) | 06-037-1103
Denver - CAMP (CO) | 08-031-0002
Chicago - Naperville-Elgin (IL) | 17-031-3103
Houston - Bayland Park (TX) | 48-201-0055
New York - Queens College (NY) | 36-081-0124
Atlanta - South DeKalb (GA) | 13-089-0002
Concentrations [ppb]
Hour in Local Time
NO
NO2
O3
HCHO
NOx
Ox

(b)

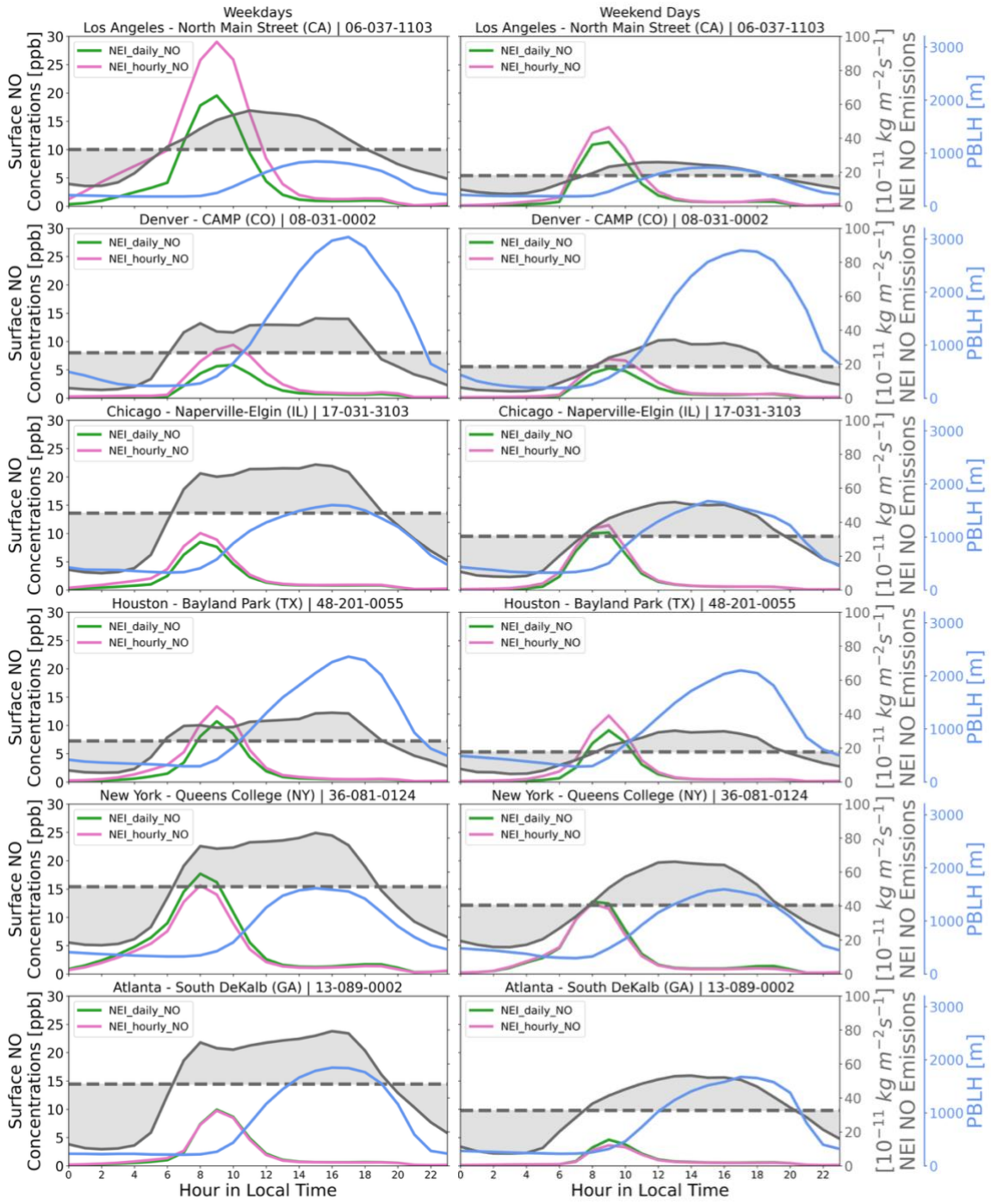

Fig. S13: Same analysis as Fig. 6 but extended to all sites and including July 2018 weekend-day averages (left column) in addition to weekday (right column). Panel (a) corresponds to Fig. 6b and shows hourly surface concentrations of NO, NO_2, O_3, and HCHO; panel (b) corresponds to Fig. 6c and shows hourly NO concentrations from *NEI_daily_NO* and *NEI_hourly_NO*, plotted with NO emissions and planetary boundary layer height (PBLH).

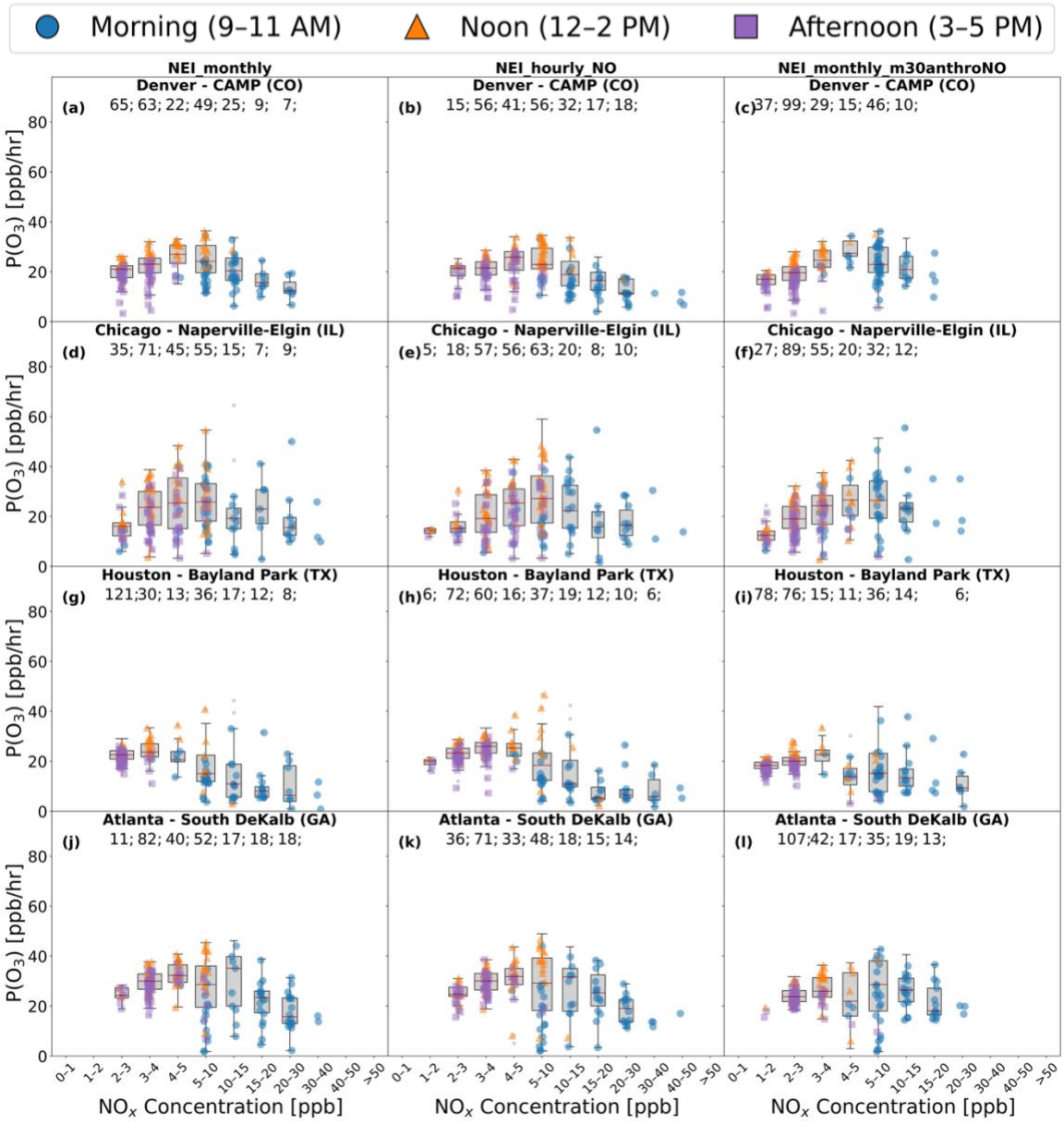

Fig. S14: Same as Fig. 7, but for sites in Denver (CO), Chicago (IL), Houston (TX), and Atlanta (GA).

Table S1. Five-day sensitivity simulations (July 1-5, 2018) used to test model responses to changes in anthropogenic and biogenic emissions and to an alternative chemical mechanism, relative to the *BASE* case.

Simulation ID	Chemical Mechanism	Nudging Strength	Simulation Period	Emissions Perturbation
CAMS_m30anthro	MOZART-TS1	12-hour	July 1-5, 2018	-30% total anthropogenic emissions
CAMS_m30bio	MOZART-TS1			-30% total biogenic emissions
CAMS_chemTS2	MOZART-TS2			No
CAMS_6HrNudge_chemTS1	MOZART-TS1	**6-hour**		No
CAMS_6HrNudge_chemTS2	MOZART-TS2			No

Table S2. Comparison of July mean modeled surface concentrations of NO_2, O_3, and CO with SLAMS observations from all available monitoring sites, and of tropospheric vertical column densities (VCD_{Trop}) of NO_2 and HCHO, and total vertical column densities (VCD_{Total}) of CO with TROPOMI. Results are shown for the *BASE*, *NEI_monthly*, and *NEI_hourly* cases (details in Table 1). Model performance is evaluated using Spearman's rank correlation coefficient (r_s), mean bias error (MBE), and root mean square error (RMSE), calculated separately for each region. These statistics correspond to the r_s and MBE values shown in Fig. 2, while this table provides a more comprehensive summary including RMSE. For MBE and RMSE, both the absolute values and the relative differences (in parentheses) are reported in this table. Surface SO_2 and $PM_{2.5}$ are included in Table S3.

	Region /Simulation ID	**West Coast**	**Mountain**	**Midwest**	**Southwest**	**Northeast**	**Southeast**
Surface NO_2 [ppb]							
r_s	*BASE*	0.57	0.75	0.75	0.44	0.58	0.72
	NEI_monthly	0.65	0.76	0.78	0.57	0.65	0.73
	NEI_hourly	0.66	0.78	0.79	0.57	0.64	0.71
MBE (%)	*BASE*	4.73 (67 %)	-0.64 (-15 %)	1.63 (32 %)	3.22 (60 %)	4.05 (61 %)	1.77 (27 %)
	NEI_monthly	-0.93 (-13 %)	-1.46 (-35 %)	-0.69 (-13 %)	-0.48 (-9.0 %)	-0.79 (-12 %)	-0.43 (-6.7 %)
	NEI_hourly	1.03 (15 %)	-0.51 (-12 %)	-0.35 (-6.9 %)	0.36 (6.8 %)	-1.33 (-20 %)	-0.80 (-12 %)
RMSE (%)	*BASE*	8.81 (124 %)	3.11 (74 %)	3.06 (60 %)	5.33 (100 %)	7.08 (106 %)	3.96 (61 %)

	NEI_monthly	4.85 (68 %)	3.27 (78 %)	2.48 (48 %)	3.02 (57 %)	3.96 (59 %)	3.40 (53 %)
	NEI_hourly	5.35 (75 %)	3.03 (72 %)	2.48 (48 %)	3.17 (59 %)	4.07 (61 %)	3.55 (55 %)
Surface O_3 [ppb]							
r_s	*BASE*	0.79	0.57	0.36	0.71	0.15	0.48
	NEI_monthly	0.81	0.56	0.47	0.81	0.52	0.50
	NEI_hourly	0.80	0.54	0.46	0.81	0.52	0.51
MBE (%)	*BASE*	9.34 (24 %)	6.04 (13 %)	13 (39 %)	12 (38 %)	9.73 (29 %)	11 (40 %)
	NEI_monthly	7.95 (21 %)	1.37 (2.9 %)	6.92 (21 %)	6.59 (21 %)	4.38 (13 %)	7.75 (27 %)
	NEI_hourly	9.08 (24 %)	2.65 (5.6 %)	6.55 (19 %)	6.71 (22 %)	3.12 (9.1 %)	6.92 (24 %)
RMSE (%)	*BASE*	14 (36 %)	8.51 (18 %)	14 (41 %)	13 (44 %)	11 (33 %)	14 (49 %)
	NEI_monthly	12 (31 %)	5.88 (12 %)	7.66 (23 %)	7.80 (25 %)	5.88 (18 %)	9.61 (34 %)
	NEI_hourly	13 (34 %)	6.68 (14 %)	7.36 (19 %)	7.89 (26 %)	5.00 (15 %)	8.83 (31 %)
Surface CO [ppb]							
r_s	*BASE*	0.11	0.10	0.36	0.22	0.33	0.16
	NEI_monthly	0.12	0.11	0.45	0.25	0.43	0.39
	NEI_hourly	0.14	0.08	0.48	0.34	0.43	0.36
MBE (%)	*BASE*	-85 (-35%)	-27 (-14%)	-71 (-28 %)	-70 (-27 %)	-44 (-18 %)	-136 (-46 %)
	NEI_monthly	-61 (-25 %)	-1.47 (-0.8 %)	-45 (-18 %)	-51 (-20 %)	-5.12 (-2.1 %)	-71 (-24 %)
	NEI_hourly	0.04 (0.02 %)	52 (28 %)	-34 (-14 %)	-30 (-12 %)	-31 (-13 %)	-90 (-31 %)
RMSE (%)	*BASE*	153 (63 %)	146 (79 %)	130 (52 %)	154 (60 %)	114 (47 %)	222 (76 %)
	NEI_monthly	148 (61 %)	153 (83 %)	111 (44 %)	138 (53 %)	112 (47 %)	185 (63 %)
	NEI_hourly	159 (65 %)	184 (99 %)	109 (43 %)	130 (50 %)	111 (46 %)	193 (66 %)
NO_2 VCD_{Trop} [molecules/cm^2]							
r_s	*BASE*	0.79	0.65	0.77	0.75	0.85	0.71
	NEI_monthly	0.69	0.61	0.75	0.74	0.83	0.70
	NEI_hourly	0.74	0.63	0.75	0.75	0.83	0.70
MBE (%)	*BASE*	-2.87e+14 (-30%)	-2.67e+14 (-29 %)	-2.62e+14 (-25 %)	-2.67e+14 (-27 %)	-3.03e+14 (-31 %)	-3.21e+14 (-32 %)
	NEI_monthly	-3.68e+14 (-39 %)	-3.49e+14 (-38 %)	-3.55e+14 (-34 %)	-3.55e+14 (-35 %)	-3.90e+14 (-39 %)	-3.88e+14 (-39 %)
	NEI_hourly	-3.30e+14 (-35 %)	-3.23e+14 (-35 %)	-3.49e+14 (-34 %)	-3.49e+14 (-35 %)	-3.97e+14 (-40 %)	-3.93e+14 (-40 %)
RMSE (%)	*BASE*	4.80e+14 (50 %)	3.30e+14 (36 %)	3.10e+14 (30 %)	3.20e+14 (32 %)	3.70e+14 (37 %)	3.60e+14 (37 %)
	NEI_monthly	5.70e+14 (60 %)	4.10e+14 (45 %)	4.00e+14 (38 %)	4.10e+14 (40 %)	4.60e+14 (47 %)	4.20e+14 (43 %)
	NEI_hourly	5.30e+14 (56 %)	3.80e+14 (42 %)	3.90e+14 (38 %)	4.00e+14 (40 %)	4.70e+14 (47 %)	4.30e+14 (43 %)
HCHO VCD_{Trop} [molecules/cm^2]							

r_s	*BASE*	0.75	0.60	0.69	0.92	0.75	0.90
	NEI_monthly	0.75	0.60	0.69	0.92	0.76	0.89
	NEI_hourly	0.75	0.60	0.68	0.92	0.75	0.90
MBE (%)	*BASE*	1.40e+15 (18 %)	2.19e+15 (28 %)	2.52e+15 (27 %)	3.73e+15 (32 %)	1.99e+15 (22 %)	2.11e+15 (23 %)
	NEI_monthly	1.16e+15 (15 %)	1.97e+15 (25 %)	2.20e+15 (23 %)	3.34e+15 (29 %)	1.64e+15 (18 %)	2.09e+15 (23 %)
	NEI_hourly	1.28e+15 (16 %)	2.05e+15 (26 %)	2.18e+15 (23 %)	3.38e+15 (29 %)	1.56e+15 (17 %)	2.02e+15 (22 %)
RMSE (%)	*BASE*	3.10e+15 (40 %)	2.90e+15 (37 %)	3.10e+15 (33 %)	4.40e+15 (39 %)	2.70e+15 (30 %)	2.90e+15 (31 %)
	NEI_monthly	3.00e+15 (38 %)	2.80e+15 (36 %)	2.80e+15 (30 %)	4.00e+15 (34 %)	2.30e+15 (26 %)	2.80e+15 (30 %)
	NEI_hourly	3.10e+15 (39 %)	2.90e+15 (37 %)	2.80e+15 (30 %)	4.00e+15 (35 %)	2.30e+15 (25 %)	2.70e+15 (29 %)
CO VCD_{Total} [molecules/cm^2]							
r_s	*BASE*	0.53	0.37	0.26	0.53	0.11	0.20
	NEI_monthly	0.53	0.36	0.28	0.52	0.12	0.13
	NEI_hourly	0.54	0.35	0.26	0.52	0.12	0.15
MBE (%)	*BASE*	-2.76e+16 (-1.8 %)	2.65e+16 (1.8 %)	-9.24e+16 (-5.4 %)	1.35e+17 (8.5 %)	-1.78e+17 (-10 %)	6.89e+16 (4.3 %)
	NEI_monthly	-3.79e+16 (-2.5 %)	4.75e+15 (0.3 %)	-1.19e+17 (-7.0 %)	1.14e+17 (7.2 %)	-1.87e+17 (-11 %)	7.63e+16 (4.8 %)
	NEI_hourly	-1.85e+16 (-1.2 %)	2.64e+16 (1.8 %)	-1.11e+17 (-6.5 %)	1.27e+17 (8.0 %)	-1.93e+17 (-11 %)	7.23e+16 (4.5 %)
RMSE (%)	*BASE*	2.60e+17 (17 %)	1.90e+17 (13 %)	2.1e+17 (12 %)	2.4e+17 (15 %)	3.30e+17 (19 %)	3.10e+17 (19 %)
	NEI_monthly	2.60e+17 (17 %)	1.80e+17 (13 %)	2.2e+17 (13 %)	2.3e+17 (14 %)	3.40e+17 (19 %)	3.20e+17 (20 %)
	NEI_hourly	2.60e+17 (17 %)	1.90e+17 (13 %)	2.1e+17 (12 %)	2.4e+17 (15 %)	3.40e+17 (19 %)	3.20e+17 (20 %)

Table S3. Same as Table S2 but for surface concentrations of SO_2 and $PM_{2.5}$. Comparison of July mean values from SLAMS observations and MUSICA model simulations across six regions.

	Region /Simulation ID	West Coast	Mountain	Midwest	Southwest	Northeast	Southeast
				Surface SO_2 [ppb]			
r_s	*BASE*	0.41	-0.09	0.00	0.14	0.32	0.13
	NEI_monthly	0.41	0.15	-0.06	-0.05	0.13	0.02
	NEI_hourly	0.43	0.11	-0.03	-0.06	0.12	-0.01
MBE (%)	*BASE*	2.71 (361 %)	0.91 (98 %)	4.99 (683 %)	2.78 (353 %)	11 (1651 %)	3.94 (861 %)
	NEI_monthly	-0.56 (-74 %)	-0.57 (-62 %)	-0.14 (-20 %)	0.04 (5.5 %)	-0.34 (-49 %)	-0.29 (-64 %)
	NEI_hourly	-0.51 (-68%)	-0.54 (-58 %)	-0.12 (-16 %)	0.15 (20 %)	-0.33 (-48 %)	-0.28 (-61 %)
RMSE (%)	*BASE*	4.66 (621 %)	3.19 (343 %)	9.52 (1303 %)	3.96 (502 %)	20 (2866 %)	7.35 (1607 %)
	NEI_monthly	1.12 (149 %)	1.14 (122 %)	1.05 (144 %)	1.66 (210 %)	0.86 (125 %)	0.81 (178 %)
	NEI_hourly	1.11 (147 %)	1.13 (122 %)	1.06 (145 %)	1.74 (221 %)	0.86 (125 %)	0.81 (178 %)
				Surface $PM_{2.5}$ [μg/m3]			
r_s	*BASE*	0.43	0.32	0.75	-0.35	0.15	0.27
	NEI_monthly	0.38	0.30	0.76	-0.26	0.06	0.39
	NEI_hourly	0.38	0.29	0.72	-0.30	0.08	0.41
MBE (%)	*BASE*	5.07 (52 %)	-2.38 (-31 %)	-1.03 (-13 %)	-2.25 (-16 %)	3.19 (36 %)	3.20 (37 %)
	NEI_monthly	4.69 (48 %)	-2.55 (-33 %)	-1.72 (-22 %)	-2.90 (-21 %)	2.20 (25 %)	2.34 (27 %)
	NEI_hourly	5.35 (55 %)	-2.14 (-27 %)	-1.31 (-16 %)	-2.61 (-19 %)	2.53 (29 %)	2.52 (29 %)
RMSE (%)	*BASE*	9.66 (99 %)	3.77 (49 %)	2.37 (30 %)	5.92 (43 %)	4.14 (47 %)	4.09 (47 %)
	NEI_monthly	9.46 (97 %)	3.87 (50 %)	2.59 (32 %)	5.89 (42 %)	3.68 (42 %)	3.11 (36 %)
	NEI_hourly	9.82 (100 %)	3.67 (47 %)	2.41 (30 %)	5.84 (42 %)	3.93 (45 %)	3.23 (37 %)

Table S4. Summary of the observational datasets used for MUSICA model evaluation. The table shows the units used in our analysis, which may differ from those in the original data sources.

Dataset/ Instrument	Variable [unit]	Data Type	Temporal Resolution	Spatial Resolution	Availability	Domain/Sites	Data Source
State and Local Monitoring Stations (SLAMS)	O_3 [ppb] NO_2 [ppb] CO [ppb] SO_2 [ppb] $PM_{2.5}$ [µg/m3]	Surface Measurement	Hourly	Not applicable	1980-Present	CONUS	AQS Air Data (https://aqs.epa.gov/aqsweb/airdata/download_files.html; access date: 8/1/2023)
Level-2 TROPOMI RPRO Version 02.04.00	HCHO [molec/cm2] and Averaging Kernels [unitless]	Tropospheric VCD Retrievals	Daily (~1:30 PM Local Time)	5.5 km x 3.5 km (Re-gridded to 0.05° × 0.05° selecting for QA>0.75)	5/7/2018-Present	Global	GES DISC (doi: 10.5270/S5P-vg1i7t0; access date: 12/1/2023)
Level-2 TROPOMI RPRO Version 02.04.00	NO_2 [molec/cm2] and Averaging Kernels [unitless]	Tropospheric VCD Retrievals	Daily (~1:30 PM Local Time)	5.5 km x 3.5 km (Re-gridded to 0.05° × 0.05° selecting for QA>0.75)	5/1/2018-Present	Global	GES DISC (doi: 10.5270/S5P-9bnp8q8; access date: 12/1/2023)
Level-2 TROPOMI RPRO Version 02.04.00	CO [molec/cm2] and Averaging Kernels [unitless]	Total VCD Retrievals	Daily (~1:30 PM Local Time)	5.5 km x 7 km (Re-gridded to 0.05° × 0.05° selecting for QA>0.75)	4/30/2018-Present	Global	GES DISC (doi: 10.5270/S5P-bj3nry0; access date: 12/1/2023)

Table S5. Geographical locations of the six selected State and Local Monitoring Stations (SLAMS) marked on Fig. 1.

City	Region	Site Name	AQS Site ID	Latitude	Longitude
Los Angeles	WestCoast	Los Angeles - North Main Street (CA)	06-037-1103	34.06659	-118.22688
Denver	Mountain	Denver - CAMP (CO)	08-031-0002	39.751184	-104.98763
Chicago	Midwest	Chicago - Naperville-Elgin (IL)	17-031-3103	41.965193	-87.876265
Houston	Southwest	Houston - Bayland Park (TX)	48-201-0055	29.695729	-95.499219
New York City	Northeast	New York - Queens College (NY)	36-081-0124	40.73614	-73.82153
Atlanta	Southeast	Atlanta - South DeKalb (GA)	13-089-0002	33.6878	-84.2905

Table S6. Regional- and city-scale statistics of estimated biases in inferred anthropogenic NO emission magnitude (%) for July 2018, calculated using model-simulated tropospheric NO_2 columns. The timing-representation bias is derived from monthly mean NO_2 columns by comparing *NEI_hourly_NO* and *NEI_monthly*, isolating the effect of unresolved diurnal emission timing. The CONUS mean is computed as the average across the six defined regions. Methodological details are provided in Text S6.

Scale	Location	Timing-representation bias (%)
	CONUS	+1.8
Region	WestCoast	+7.7
	Mountain	+5.4
	Midwest	+0.6
	Southwest	+1.5
	Northeast	-2.8
	Southeast	-2.4
City	Los Angeles	+26
	Denver	+30
	Chicago	+7.1
	Houston	+12
	New York	-6.8
	Atlanta	-4.1

REFERENCES

Davis, N. A., Callaghan, P., Simpson, I. R., and Tilmes, S.: Specified Dynamics Scheme Impacts on Wave-Mean Flow Dynamics, Convection, and Tracer Transport in CESM2 (WACCM6), Atmos. Chem. Phys., 22, 197–214, https://doi.org/10.5194/acp-22-197-2022, 2022.

Gaubert, B., Emmons, L. K., Raeder, K., Tilmes, S., Miyazaki, K., Arellano Jr., A. F., Elguindi, N., Granier, C., Tang, W., Barré, J., Worden, H. M., Buchholz, R. R., Edwards, D. P., Franke, P., Anderson, J. L., Saunois, M., Schroeder, J., Woo, J.-H., Simpson, I. J., Blake, D. R., Meinardi, S., Wennberg, P. O., Crounse, J., Teng, A., Kim, M., Dickerson, R. R., He, H., Ren, X., Pusede, S. E., and Diskin, G. S.: Correcting Model Biases of CO in East Asia: Impact on Oxidant Distributions During Korus-Aq KORUS-AQ, Atmos. Chem. Phys., 20, 14617–14647, https://doi.org/10.5194/acp-20-14617-2020, 2020.

Keller, C. A., Long, M. S., Yantosca, R. M., Da Silva, A. M., Pawson, S., and Jacob, D. J.: HEMCO v1.0: A Versatile, ESMF-compliant Component for Calculating Emissions in Atmospheric Models, Geosci. Model Dev., 7, 1409–1417, https://doi.org/10.5194/gmd-7-1409-2014, 2014.

Lamsal, L. N., Krotkov, N. A., Celarier, E. A., Swartz, W. H., Pickering, K. E., Bucsela, E. J., Gleason, J. F., Martin, R. V., Philip, S., Irie, H., Cede, A., Herman, J., Weinheimer, A., Szykman, J. J., and Knepp, T. N.: Evaluation of OMI Operational Standard NO_2 Column Retrievals Using in Situ and Surface-Based NO_2 Observations, Atmos. Chem. Phys., 14, 11587–11609, https://doi.org/10.5194/acp-14-11587-2014, 2014.

Li, J., Yu, S., Chen, X., Zhang, Y., Li, M., Li, Z., Song, Z., Liu, W., Li, P., Xie, M., and Xing, J.: Evaluation of the WRF-CMAQ Model Performances on Air Quality in China with the Impacts of the Observation Nudging on Meteorology, Aerosol Air Qual. Res., 22, 220023, https://doi.org/10.4209/aaqr.220023, 2022.

Lin, H., Jacob, D. J., Lundgren, E. W., Sulprizio, M. P., Keller, C. A., Fritz, T. M., Eastham, S. D., Emmons, L. K., Campbell, P. C., Baker, B., Saylor, R. D., and Montuoro, R.: Harmonized Emissions Component (HEMCO) 3.0 as a Versatile Emissions Component for Atmospheric Models: Application in the GEOS-Chem, NASA GEOS, WRF-GC, CESM2, NOAA GEFS-Aerosol, and NOAA UFS Models, Geosci. Model Dev., 14, 5487–5506, https://doi.org/10.5194/gmd-14-5487-2021, 2021.

van Noije, T. P. C., Eskes, H. J., van Weele, M., and van Velthoven, P. F. J.: Implications of the Enhanced Brewer-Dobson Circulation in European Centre for Medium-Range Weather Forecasts Reanalysis Era-40 for the Stratosphere-Troposphere Exchange of Ozone in Global Chemistry Transport Models, Journal of Geophysical Research: Atmospheres, 109, https://doi.org/https://doi.org/10.1029/2004JD004586, 2004.

Otte, T. L.: The Impact of Nudging in the Meteorological Model for Retrospective Air Quality Simulations. Part I: Evaluation against National Observation Networks, J. Appl. Meteorol. Climatol., 47, 1853–1867, https://doi.org/https://doi.org/10.1175/2007JAMC1790.1, 2008.

Schwantes, R. H., Lacey, F. G., Tilmes, S., Emmons, L. K., Lauritzen, P. H., Walters, S., Callaghan, P., Zarzycki, C. M., Barth, M. C., Jo, D. S., Bacmeister, J. T., Neale,

R. B., Vitt, F., Kluzek, E., Roozitalab, B., Hall, S. R., Ullmann, K., Warneke, C., Peischl, J., Pollack, I. B., Flocke, F., Wolfe, G. M., Hanisco, T. F., Keutsch, F. N., Kaiser, J., Bui, T. P. V, Jimenez, J. L., Campuzano-Jost, P., Apel, E. C., Hornbrook, R. S., Hills, A. J., Yuan, B., and Wisthaler, A.: Evaluating the Impact of Chemical Complexity and Horizontal Resolution on Tropospheric Ozone Over the Conterminous US With a Global Variable Resolution Chemistry Model, J. Adv. Model. Earth Syst., 14, e2021MS002889, https://doi.org/https://doi.org/10.1029/2021MS002889, 2022.

Turnock, S. T., Wild, O., Dentener, F. J., Davila, Y., Emmons, L. K., Flemming, J., Folberth, G. A., Henze, D. K., Jonson, J. E., Keating, T. J., Kengo, S., Lin, M., Lund, M., Tilmes, S., and O'Connor, F. M.: The Impact of Future Emission Policies on Tropospheric Ozone Using a Parameterised Approach, Atmos. Chem. Phys., 18, 8953–8978, https://doi.org/10.5194/acp-18-8953-2018, 2018.

Wild, O., Fiore, A. M., Shindell, D. T., Doherty, R. M., Collins, W. J., Dentener, F. J., Schultz, M. G., Gong, S., MacKenzie, I. A., Zeng, G., Hess, P., Duncan, B. N., Bergmann, D. J., Szopa, S., Jonson, J. E., Keating, T. J., and Zuber, A.: Modelling Future Changes in Surface Ozone: A Parameterized Approach, Atmos. Chem. Phys., 12, 2037–2054, https://doi.org/10.5194/acp-12-2037-2012, 2012.

Wu, S., Duncan, B. N., Jacob, D. J., Fiore, A. M., and Wild, O.: Chemical Nonlinearities in Relating Intercontinental Ozone Pollution to Anthropogenic Emissions, Geophys. Res. Lett., 36, https://doi.org/https://doi.org/10.1029/2008GL036607, 2009.